

Article

Fault Detection and Fault-Tolerant Cooperative Control of Multi-UAVs under Actuator Faults, Sensor Faults, and Wind Disturbances

Zhongyu Yang ¹, Mengna Li ¹, Ziquan Yu ¹, Yuehua Cheng ¹, Guili Xu ¹ and Youmin Zhang ^{2,*}

¹ College of Automation Engineering, Nanjing University of Aeronautics and Astronautics, Nanjing 211106, China; yangzhongyu@nuaa.edu.cn (Z.Y.); limengna@nuaa.edu.cn (M.L.); yuziquan@nuaa.edu.cn (Z.Y.); chengyuehua@nuaa.edu.cn (Y.C.); guilixu@nuaa.edu.cn (G.X.)

² Mechanical, Industrial and Aerospace Engineering, Concordia University, Montreal, QC H3G 1M8, Canada

* Correspondence: ymzhang@encs.concordia.ca

Abstract: Fault detection (FD) and fault-tolerant cooperative control (FTCC) strategies are proposed in this paper for multiple fixed-wing unmanned aerial vehicles (UAVs) under actuator faults, sensor faults, and wind disturbances. Firstly, the faulty model is introduced while the effectiveness loss, deviation of thrust throttle setting, and pitot sensor faults are considered. Secondly, the faulty UAV model with wind disturbances is linearized and the system is then converted into two subsystems by using state and output transformations. Further, cooperative unknown input observers (UIOs) are developed to estimate the faults, disturbances, and states. By combining with the observers' estimations, adaptive thresholds are designed to detect actuator and sensor faults in the system. Then, considering state constraints, a backstepping-based FTCC scheme is proposed for multiple UAVs (multi-UAVs) suffering from actuator faults, sensor faults, and wind disturbances. It is shown by Lyapunov analysis that the tracking errors are fixed-time convergent. Finally, the effectiveness of the FD and FTCC scheme is verified by numerical simulation.

Keywords: fault detection; fault-tolerant cooperative control; sensor fault; actuator fault; wind disturbance



Citation: Yang, Z.; Li, M.; Yu, Z.; Cheng, Y.; Xu, G.; Zhang, Y. Fault Detection and Fault-Tolerant Cooperative Control of Multi-UAVs under Actuator Faults, Sensor Faults, and Wind Disturbances. *Drones* **2023**, *7*, 503. <https://doi.org/10.3390/drones7080503>

Academic Editor: Mostafa Hassanalian

Received: 3 July 2023

Revised: 24 July 2023

Accepted: 27 July 2023

Published: 1 August 2023



Copyright: © 2023 by the authors. Licensee MDPI, Basel, Switzerland. This article is an open access article distributed under the terms and conditions of the Creative Commons Attribution (CC BY) license (<https://creativecommons.org/licenses/by/4.0/>).

1. Introduction

Due to low cost and flexible deployment characteristics, unmanned aerial vehicles (UAVs) have been increasingly, and more widely, used in numerous fields, such as forest fire monitoring [1,2], search and rescue [3], and power grid inspection [4]. Among these uses, fixed-wing UAVs have been widely used in wide-area coverage search [5], long-distance logistics transportation [6], and communication relays [7], due to their strong carrying capacity, fast flight speed, and long endurance.

With the development of UAV autonomous technology, cooperative control of multiple UAVs (multi-UAVs) has become an important research direction [8–12]. Through cooperative operations, multi-UAVs demonstrate high task execution efficiency, superior coordination, intelligence, and autonomy. To ensure the cooperative control performance of multi-UAV systems during mission execution, operational safety has become a hot research issue in the field of flight control. When multi-UAVs cooperate in performing tasks, such as environmental monitoring, fire monitoring, and collaborative search, there is a risk of losing control of the faulty UAVs if one or more UAVs encounter physical faults. In severe cases, the faulty UAVs may collide with surrounding UAVs, resulting in the entire flight formation losing control. Therefore, studying the problem of fault detection (FD), fault estimation, and fault-tolerant cooperative control (FTCC) is of great theoretical significance and practical necessity for the safe flight of monitoring missions and the safe control of multi-UAV systems.

It is worth noting that, with increases in operating time, environmental complexity, and severity, actuators and sensors may experience wear and aging. Furthermore, in the cooperative formation flight of multi-UAVs, the number of system components in the entire system significantly increases. The multi-UAVs system involves communication network connections, which provide the faulty UAVs with the opportunity to send perturbed state information to all nearby UAVs, greatly increasing the probability of collision and failure of the mission undertaken. Compared with the FD and fault-tolerant control (FTC) for single UAVs, the FD and FTCC for multi-UAVs are increasingly complicated. In addition, the external disturbances encountered by UAVs and the system nonlinearity also pose great challenges and difficulties in researching multi-UAVs. How to detect various faults in a multi-UAV system affected by disturbances, and to deal with the faults effectively, have become significant research topics to ensure the safe and cooperative formation flight of multi-UAVs.

In order to discover faults in the system in a timely and accurate manner, many scholars have carried out extensive research on this topic [13–16]. In [17], two sensor fault estimation schemes were proposed for a class of nonlinear systems with uncertainties, which were then applied to satellite control systems. The incipient fault diagnosis of a class of Lipschitz nonlinear systems was studied in [18]. By constructing total measurable fault information residual (ToMFIR), the incipient faults of multiple sensors can be detected. The linear descriptor reduced-order observer and descriptor sliding-mode observer were proposed to solve the state and fault estimation problems of linear systems with disturbances, sensor and actuator faults in [19]. Nevertheless, the FD results on multi-UAV systems with actuators and sensor faults and disturbances are very rare.

In practical situations, the consideration of a state constraint is very important for UAVs, since this consideration can simultaneously prevent the occurrence of accidents, ensure the safety of UAVs, improve system stability, enhance performance and efficiency, and reduce energy consumption during flight. In recent years, some methods have been proposed in regard to constraint control problems, including the invariant-set method [20,21], model predictive control (MPC) [22,23], and barrier Lyapunov function (BLF) [24,25], etc. A distributed FTC method and state transformations with the scaling function were proposed for fixed-wing UAVs subject to actuator faults and full state constraints, maintaining speed and attitude within the corresponding constraint ranges [26]. In [27], an adaptive FTC scheme, based on reinforcement learning and barrier Lyapunov control technology, was designed to solve the attitude tracking problem of flying-wing UAVs under actuator fault, actuator saturation, and attitude angle constraints. A novel integral barrier Lyapunov function (IBLF) was proposed for the FTC of fixed-wing UAVs with asymmetric time-varying full state constraints [28]. Nevertheless, the state constraint problem of multiple fixed-wing UAVs is rarely considered, which needs further investigations.

To better improve the cooperative operation performance of the entire multi-UAV system, numerous researchers have achieved a quantity of exploratory FTCC results. At present, FTCC schemes are mainly developed based on the leader–follower formation [29–31] and distributed communication architectures [32–34]. In [35], a dynamic surface fixed-time FTC scheme, based on a neoteric disturbance observer, was proposed for fixed-wing UAVs against actuator faults and external disturbances. A fault detection observer was proposed by using the H_∞ method for sensor faults in a multi-UAV system. Then, a distributed fault-tolerant formation controller was designed in [36]. In [37], by using intelligent learning architecture and fractional-order calculus, an FTCC strategy was proposed for multiple fixed-wing UAVs with actuator and sensor faults. In addition, there is a high demand to design fixed-time FTCC schemes to ensure rapid fault tolerance.

Based on the above discussions, in this paper, the FD and FTCC strategy are proposed to solve the cooperative control problem of multiple fixed-wing UAVs with actuator faults, sensor faults, and wind disturbances. The contributions of this paper are mainly as follows.

1. Compared with the previous results on FD and fault estimation methods in [17–19], a newly constructed cooperative unknown input observer (UIO) is developed to

- estimate states, faults, and disturbances. Combined with the observers' estimations, adaptive thresholds are designed to detect actuator and sensor faults in the system.
2. Tangential barrier Lyapunov function (TBLF) is combined with the state transformation with scaling function to constrain the states.
 3. Differing from existing FTC strategies for fixed-wing UAVs [35–37], a backstepping-based fixed-time FTCC scheme is proposed for multi-UAVs suffering from actuator faults, sensor faults, and wind disturbances.

The rest of this paper is organized as follows. Section 2 introduces the fixed-wing UAV models with wind disturbances, actuator fault, sensor fault, and the preliminaries for controller design. FD and fault estimation schemes are proposed in Section 3. An FTCC scheme is designed in Section 4. Section 5 illustrates the simulation results. Conclusions are presented in Section 6.

2. Preliminaries and Problem Statement

2.1. UAV Dynamics

In this paper, a group of fixed-wing follower UAVs and a virtual leader are considered. The dynamic model of the follower UAV# i with wind disturbances is given as follows [38]:

$$\begin{cases} \dot{x}_i = V_i \cos \gamma_i \cos \chi_i + W_x \\ \dot{y}_i = V_i \cos \gamma_i \sin \chi_i + W_y \\ \dot{z}_i = V_i \sin \gamma_i + W_z \end{cases} \quad (1)$$

where $p_i = [x_i, y_i, z_i]^T$ is the position of the UAV# i in the inertial frame for $i \in \{1, 2, \dots, N\}$. V_i , χ_i , and γ_i denote the velocity, heading angle, and flight path angle, respectively. W_x , W_y , and W_z are the components of the wind speed vector along the x , y and z axes of the inertial coordinate system.

The force equations are expressed as:

$$\begin{cases} \dot{V}_i = (-D_i + T_i)/m - g \sin \gamma_i - \dot{W}_x \cos \gamma_i \cos \chi_i - \dot{W}_y \cos \gamma_i \sin \chi_i - \dot{W}_z \sin \gamma_i \\ \dot{\chi}_i = L_i \sin \phi_i / m V_i \cos \gamma_i + (\dot{W}_x \sin \chi_i - \dot{W}_y \cos \chi_i) / V_i \cos \gamma_i \\ \dot{\gamma}_i = L_i \cos \phi_i / m V_i - mg \cos \gamma_i / V_i + (\dot{W}_x \sin \gamma_i \cos \chi_i + \dot{W}_y \sin \gamma_i \sin \chi_i - \dot{W}_z \cos \gamma_i) / V_i \end{cases} \quad (2)$$

where m and g are the mass and gravitational constant, respectively. T_i , D_i , and L_i represent the thrust, drag, and lift forces, respectively. ϕ_i denotes the bank angle.

The forces T_i and D_i are described as:

$$\begin{cases} T_i = T_{max} \delta_{ti} \\ D_i = \bar{q}_i s_i C_{iD0} \end{cases} \quad (3)$$

where T_{max} and δ_{ti} denote the maximal engine thrust force and instantaneous thrust throttle setting, respectively. The value $\bar{q}_i = 1/2\rho V_i^2$ denotes the the dynamic pressure and ρ is the air density, s_i denotes the wing area. C_{iD0} is the aerodynamic coefficient.

Define $x_{1i} = [x_i, y_i, h_i]^T$, $x_{2i} = [V_i, \chi_i, \gamma_i]^T$, $u_i = [\delta_{ti}, \phi_i, L_i]^T$, one has:

$$\begin{cases} \dot{x}_{1i} = F_{1i} + G_{1i}x_{2i} + W_i \\ \dot{x}_{2i} = F_{2i} + G_{2i}u_i + \bar{W}_i \end{cases} \quad (4)$$

where F_{1i} , G_{1i} , F_{2i} , G_{2i} , W_i , \bar{W}_i are given as

$$F_{1i} = \begin{bmatrix} V_i \cos \gamma_i \cos \chi_i - V_i \\ V_i \cos \gamma_i \sin \chi_i - \chi_i \\ V_i \sin \gamma_i - \gamma_i \end{bmatrix}, G_{1i} = \begin{bmatrix} 1 & 0 & 0 \\ 0 & 1 & 0 \\ 0 & 0 & 1 \end{bmatrix},$$

$$\begin{aligned}
 \mathbf{F}_{2i} &= \begin{bmatrix} -D_i/m - g \sin \gamma_i \\ (L_i \sin \phi_i)/(mV_i \cos \gamma_i) - \phi_i \\ (L_i \cos \phi_i)/(mV_i) - g \cos \gamma_i/V_i - L_i \end{bmatrix}, \mathbf{G}_{2i} = \begin{bmatrix} T_{\max}/m & 0 & 0 \\ 0 & 1 & 0 \\ 0 & 0 & 1 \end{bmatrix}, \\
 \mathbf{W}_i &= \begin{bmatrix} W_x \\ W_y \\ W_z \end{bmatrix}, \bar{\mathbf{W}}_i = \begin{bmatrix} -\dot{W}_x \cos \gamma_i \cos \chi_i - \dot{W}_y \cos \gamma_i \sin \chi_i - \dot{W}_z \sin \gamma_i \\ (\dot{W}_x \sin \chi_i - \dot{W}_y \cos \chi_i)/V_i \cos \gamma_i \\ (\dot{W}_x \sin \gamma_i \cos \chi_i + \dot{W}_y \sin \gamma_i \sin \chi_i - \dot{W}_z \cos \gamma_i)/V_i \end{bmatrix}.
 \end{aligned}$$

2.2. Faulty UAV Model

Actuator and sensor faults may give rise to the degradation of flight performance and affect the safety of the formation team. The thrust output of the engine may differ from the expected value due to wear or fault of the engine. Pitot may be faulty due to environmental erosion or influence. For the above reasons, we considered the effectiveness loss, deviation of thrust throttle setting, and pitot faults in this paper, given as $\delta_{ti} = \rho_{ti}\delta_{t0i} + \delta_{tbi}$ and $V_{si} = \varrho_{vi}V_i + V_{bi}$. Thus, the following fault models are obtained [37]:

$$\begin{aligned}
 \mathbf{u}_i &= \rho_i \mathbf{u}_{0i} + \mathbf{u}_{bi} \\
 &= \mathbf{u}_{0i} + \mathbf{f}_{ai}
 \end{aligned} \tag{5}$$

where \mathbf{u}_i and $\mathbf{u}_{0i} = [u_{01i}, u_{02i}, u_{03i}]^T$ denote the applied and commanded control input signals, respectively. $\rho_i = \text{diag}\{\rho_{ti}, 1, 1\}$, $\rho_{ti} \in (0, 1]$ denotes the control effectiveness. $\mathbf{u}_{bi} = [\delta_{tbi}, 0, 0]^T$ denotes the deviation value. $\mathbf{f}_{ai} = (\rho_i - \mathbf{I})\mathbf{u}_{0i} + \mathbf{u}_{bi} = [f_{a1i}, f_{a2i}, f_{a3i}]^T$.

$$\begin{aligned}
 \check{\mathbf{x}}_{2i} &= \varrho_i \mathbf{x}_{2i} + \mathbf{x}_{bi} \\
 &= \mathbf{x}_{2i} + \mathbf{f}_{si}
 \end{aligned} \tag{6}$$

where $\check{\mathbf{x}}_{2i}$ and \mathbf{x}_{2i} denote the measured and real state signals, respectively. $\varrho_i = \text{diag}\{\varrho_{vi}, 1, 1\}$, $\varrho_{vi} \in (0, 1]$ denotes the measurement effectiveness. $\mathbf{x}_{bi} = [V_{bi}, 0, 0]^T$ denotes the deviation value. $\mathbf{f}_{si} = (\varrho_i - \mathbf{I})\mathbf{x}_{2i} + \mathbf{x}_{bi} = [f_{s1i}, f_{s2i}, f_{s3i}]^T$.

By substituting (5) and (6) into (4), the faulty UAV model is presented as:

$$\begin{cases} \dot{\mathbf{x}}_{1i} = \mathbf{F}_{1i} + \mathbf{G}_{1i}[\check{\mathbf{x}}_{2i} - (\varrho_i - \mathbf{I})\mathbf{x}_{2i} - \mathbf{x}_{bi}] + \mathbf{W}_i \\ \dot{\check{\mathbf{x}}}_{2i} = \mathbf{F}_{2i} + \mathbf{G}_{2i}(\rho_i \mathbf{u}_{0i} + \mathbf{u}_{bi}) + (\varrho_i - \mathbf{I})(\mathbf{F}_{2i} + \mathbf{G}_{2i}(\rho_i \mathbf{u}_{0i} + \mathbf{u}_{bi})) + \varrho_i \mathbf{x}_{2i} + \dot{\mathbf{x}}_{bi} + \bar{\mathbf{W}}_i \end{cases} \tag{7}$$

2.3. Communication Network

Leader and N follower UAVs were considered in the multi-UAV system. The communication network among the follower UAVs is presented by an undirected topology $\mathcal{G} \triangleq (v, \varepsilon)$, where $v = \{1, 2, \dots, N\}$ is a set of follower UAVs and $\varepsilon \subseteq v \times v$ is an edge set. If $(i, j) \in \varepsilon$, the j th UAV is a neighbor of the i th UAV. $\Omega_i = \{j \in v | (i, j) \in \varepsilon\}$ is the neighborhood set of the i th UAV. The adjacency matrix $\mathcal{A} = [a_{ij}] \in \mathbb{R}^{N \times N}$ is given by $a_{ij} = 1$ if $(i, j) \in \varepsilon$ and $a_{ij} = 0$ otherwise. The Laplacian matrix $\mathcal{L} \triangleq \mathcal{D} - \mathcal{A}$, where $\mathcal{D} = \text{diag}(\Gamma_i) \in \mathbb{R}^{N \times N}$ with $\Gamma_i = \sum_{j \in \Omega_i} a_{ij}$. Furthermore, the leader adjacency matrix $\mathcal{C} = \text{diag}\{c_1, c_2, \dots, c_N\}$ is given by $c_i = 1$ if the i th UAV can obtain the information of the leader and $c_i = 0$ otherwise.

2.4. Control Objective

FD and FTCC scheme for multiple fixed-wing UAVs against actuator faults, sensor faults and wind disturbances are proposed in this paper and the objectives are listed as follows: (a) The actuator faults and sensor faults to be detected by the fault detection scheme; (b) The faults and wind disturbances to be estimated by the developed cooperative UIOs; (c) The desired cooperative formation flight can be kept by the designed FTCC scheme.

The following assumptions and lemmas may be used for the FD and FTCC designs.

Assumption 1. *The communication network of multi-UAVs system is undirected and connected.*

Lemma 1 ([39]). Consider the system $\dot{x} = f(x(t))$, $x(0) = x_0$. If there exists a Lyapunov function $V(x)$ and constants $\alpha > 0$, $\beta > 0$, $p > 1$, $0 < q < 1$, and $0 < \varpi < \infty$ such that:

$$\dot{V}(x) \leq -\alpha V^p(x) - \beta V^q(x) + \varpi \tag{8}$$

Then, the system is practically fixed-time stable. The settling time T is presented as $T \leq T_{\max} = \frac{1}{\alpha\phi(p-1)} + \frac{1}{\beta\phi(1-q)}$ with $0 < \phi < 1$. The convergence neighborhood is given by:

$$x \in \left\{ V(x) \leq \min \left\{ \left(\frac{\varpi}{(1-\phi)\alpha} \right)^{\frac{1}{p}}, \left(\frac{\varpi}{(1-\phi)\beta} \right)^{\frac{1}{q}} \right\} \right\}.$$

3. Fault Detection and Estimation Scheme Design

By using the feedback linearization, the fixed-wing UAV model (1)–(2) in the presence of actuator and sensor faults can be rewritten as:

$$\begin{cases} \dot{X}_i(t) = AX_i(t) + Bu_{0i}(t) + M\eta_i(t, X_i, u_{0i}) + Dd_i(t, X_i) + Ef_{a1i}(t) \\ y_i(t) = CX_i(t) + Ff_{s1i}(t) \end{cases} \tag{9}$$

where $X_i = [x_i, y_i, h_i, V_i, \chi_i, \gamma_i]^T$ represents the state variable, $u_{0i} = [\delta_{ti}, \phi_i, L_i]^T$ denotes the input signal, $y_i = [h_i, V_i]^T$ is output vector. $\eta_i(t, X_i, u_{0i})$ denotes the nonlinear term, which satisfies the Lipschitz constraints in Assumption 2. $d_i(t, X_i)$ represents external disturbance. $f_{a1i}(t)$ and $f_{s1i}(t)$ are actuator fault signals and sensor fault signals, respectively. A, B, C, D, E, F , and M are constant matrices. $\eta_i(t, X_i, u_{0i})$, $d_i(t, X_i)$, and the constant matrices are given as:

$$\eta_i = \begin{bmatrix} V_i \cos \gamma_i \cos \chi_i - V_i \\ V_i \cos \gamma_i \sin \chi_i - \chi_i \\ V_i \sin \gamma_i - \gamma_i \\ -D_i/m - g \sin \gamma_i \\ (L_i \sin \phi_i)/(mV_i \cos \gamma_i) - \phi_i \\ (L_i \cos \phi_i)/(mV_i) - g \cos \gamma_i/V_i - L_i \end{bmatrix}, A = \begin{bmatrix} 0 & 0 & 0 & 1 & 0 & 0 \\ 0 & 0 & 0 & 0 & 1 & 0 \\ 0 & 0 & 0 & 0 & 0 & 1 \\ 0 & 0 & 0 & 0 & 0 & 0 \\ 0 & 0 & 0 & 0 & 0 & 0 \\ 0 & 0 & 0 & 0 & 0 & 0 \end{bmatrix}, E = \begin{bmatrix} 0 \\ 0 \\ 0 \\ \frac{T_{\max}}{m} \\ 0 \\ 0 \end{bmatrix},$$

$$d_i = \begin{bmatrix} W_x \\ W_y \\ W_z \\ -\dot{W}_x \cos \gamma_i \cos \chi_i - \dot{W}_y \cos \gamma_i \sin \chi_i - \dot{W}_z \sin \gamma_i \\ (\dot{W}_x \sin \chi_i - \dot{W}_y \cos \chi_i)/(V_i \cos \gamma_i) \\ (\dot{W}_x \sin \gamma_i \cos \chi_i + \dot{W}_y \sin \gamma_i \sin \chi_i - \dot{W}_z \cos \gamma_i)/V_i \end{bmatrix}, C = \begin{bmatrix} 0 & 0 & 1 & 0 & 0 & 0 \\ 0 & 0 & 0 & 1 & 0 & 0 \end{bmatrix},$$

$$B = \begin{bmatrix} 0 & 0 & 0 \\ 0 & 0 & 0 \\ 0 & 0 & 0 \\ \frac{T_{\max}}{m} & 0 & 0 \\ 0 & 1 & 0 \\ 0 & 0 & 1 \end{bmatrix}, D = \begin{bmatrix} 1 & 0 & 0 & 0 & 0 & 0 \\ 0 & 1 & 0 & 0 & 0 & 0 \\ 0 & 0 & 1 & 0 & 0 & 0 \\ 0 & 0 & 0 & 1 & 0 & 0 \\ 0 & 0 & 0 & 0 & 1 & 0 \\ 0 & 0 & 0 & 0 & 0 & 1 \end{bmatrix}, F = \begin{bmatrix} 0 \\ 1 \end{bmatrix}, M = \begin{bmatrix} 1 & 0 & 0 & 0 & 0 & 0 \\ 0 & 1 & 0 & 0 & 0 & 0 \\ 0 & 0 & 1 & 0 & 0 & 0 \\ 0 & 0 & 0 & 1 & 0 & 0 \\ 0 & 0 & 0 & 0 & 1 & 0 \\ 0 & 0 & 0 & 0 & 0 & 1 \end{bmatrix}.$$

The nominal form of system (1)–(2) can be written as:

$$\begin{cases} \dot{X}_{Ni}(t) = AX_{Ni}(t) + Bu_{N0i}(t) + M\eta_i(t, X_{Ni}, u_{N0i}) + Dd_i(t, X_{Ni}) \\ y_{Ni}(t) = CX_{Ni}(t) \end{cases} \tag{10}$$

Assumption 2. The nonlinear term $\eta_i(t, X_i, u_{0i})$ is assumed to be Lipschitz about x locally, i.e., $\forall \|X_{1i}\| \leq \bar{X}, \|X_{2i}\| \leq \bar{X}$,

$$\|\eta_i(t, X_{1i}, u_{0i}) - \eta_i(t, X_{2i}, u_{0i})\| \leq L_p \|X_{1i} - X_{2i}\| \tag{11}$$

where \bar{X} is a positive constant. L_p is the Lipschitz constant.

Considering the influence of disturbances $d_i(t, X_i)$ on FD, linear non-singular transformation is carried out for the system (9) to realize the decoupling of disturbances and faults. Therefore, the introduced state and output transformation matrices T and S satisfy [18]:

$$\begin{cases} X_i(t) = T^{-1}z_i(t) = T^{-1} \begin{bmatrix} z_{1i}(t) \\ z_{2i}(t) \end{bmatrix} \\ y_i(t) = S^{-1}v_i(t) = S^{-1} \begin{bmatrix} v_{1i}(t) \\ v_{2i}(t) \end{bmatrix} \end{cases} \tag{12}$$

where $T^{-1} \in \mathbb{R}^{6 \times 6}$, $S^{-1} \in \mathbb{R}^{2 \times 2}$, $z_{1i}(t) \in \mathbb{R}^3$, $z_{2i}(t) \in \mathbb{R}^3$.

According to (9) and (12), one obtains

$$\begin{cases} \dot{z}_i(t) = TAT^{-1}z_i(t) + TM\eta_i(t, T^{-1}z_i, u_{0i}) + TBu_{0i}(t) + TDd_i(t, T^{-1}z_i) + TEf_{a1i}(t) \\ \bar{v}_i(t) = SCT^{-1}z_i(t) + SFf_{s1i}(t) \end{cases} \tag{13}$$

Further, it can be obtained from (13) that:

$$\begin{cases} \dot{z}_i(t) = \bar{A}z_i(t) + \bar{B}u_{0i}(t) + \bar{M}\eta_i(t, T^{-1}z_i, u_{0i}) + \bar{D}d_i(t, T^{-1}z_i) + \bar{E}f_{a1i}(t) \\ \bar{v}_i(t) = \bar{C}z_i(t) + \bar{F}f_{s1i}(t) \end{cases} \tag{14}$$

where $\bar{A} = TAT^{-1} = \begin{bmatrix} \bar{A}_{11} & \bar{A}_{12} \\ \bar{A}_{21} & \bar{A}_{22} \end{bmatrix} \in \mathbb{R}^{6 \times 6}$, $\bar{A}_{11} \in \mathbb{R}^{3 \times 3}$, $\bar{A}_{12} \in \mathbb{R}^{3 \times 3}$, $\bar{A}_{21} \in \mathbb{R}^{3 \times 3}$, $\bar{A}_{22} \in \mathbb{R}^{3 \times 3}$. $\bar{B} = TB = \begin{bmatrix} \bar{B}_1 \\ \bar{B}_2 \end{bmatrix} \in \mathbb{R}^{6 \times 3}$, $\bar{B}_1 \in \mathbb{R}^{3 \times 3}$, $\bar{B}_2 \in \mathbb{R}^{3 \times 3}$. $\bar{M} = TM = \begin{bmatrix} \bar{M}_1 \\ \bar{M}_2 \end{bmatrix} \in \mathbb{R}^{6 \times 6}$, $\bar{M}_1 \in \mathbb{R}^{3 \times 6}$, $\bar{M}_2 \in \mathbb{R}^{3 \times 6}$. $\bar{D} = TD = \begin{bmatrix} \bar{D}_1 \\ \bar{D}_2 \end{bmatrix} \in \mathbb{R}^{6 \times 6}$, $\bar{D}_1 \in \mathbb{R}^{3 \times 6}$, $\bar{D}_2 \in \mathbb{R}^{3 \times 6}$. $\bar{E} = TE = \begin{bmatrix} \mathbf{0} \\ \bar{E}_2 \end{bmatrix} \in \mathbb{R}^{6 \times 1}$, $\bar{E}_2 \in \mathbb{R}^{3 \times 1}$. $\bar{C} = SCT^{-1} = \begin{bmatrix} \bar{C}_{11} & \mathbf{0} \\ \mathbf{0} & \bar{C}_{22} \end{bmatrix} \in \mathbb{R}^{2 \times 6}$, $\bar{C}_{11} \in \mathbb{R}^{1 \times 3}$, $\bar{C}_{22} \in \mathbb{R}^{1 \times 3}$. $\bar{F} = SF = \begin{bmatrix} \mathbf{0} \\ \bar{F}_2 \end{bmatrix} \in \mathbb{R}^{2 \times 1}$, $\bar{F}_2 \in \mathbb{R}^{1 \times 1}$.

So far, based on (12) and (14), system (9) can be written into the following two subsystem forms after linear non-singular transformation:

$$\begin{cases} \dot{z}_{1i}(t) = \bar{A}_{11}z_{1i}(t) + \bar{A}_{12}z_{2i}(t) + \bar{B}_1u_{0i}(t) + \bar{M}_1\eta_i(t, T^{-1}z_i, u_{0i}) + \bar{D}_1d_i(t, T^{-1}z_i) \\ \bar{v}_{1i}(t) = \bar{C}_{11}z_{1i}(t) \end{cases} \tag{15}$$

$$\begin{cases} \dot{z}_{2i}(t) = \bar{A}_{21}z_{1i}(t) + \bar{A}_{22}z_{2i}(t) + \bar{B}_2u_{0i}(t) + \bar{M}_2\eta_i(t, T^{-1}z_i, u_{0i}) \\ \quad + \bar{D}_2d_i(t, T^{-1}z_i) + \bar{E}_2f_{a1i}(t) \\ \bar{v}_{2i}(t) = \bar{C}_{22}z_{2i}(t) + \bar{F}_2f_{s1i}(t) \end{cases} \tag{16}$$

According to [18,40], appropriate first-order low-pass filters are designed as (17) and (18) for subsystems to convert sensor faults into pseudo-actuator faults. Then, the output v_{1i} and v_{2i} of subsystems shown in (15) and (16) are passed through the following filters, respectively:

$$\dot{z}_{3i}(t) = A_1z_{3i}(t) + \bar{C}_{11}z_{1i}(t) = A_1z_{3i}(t) + v_{1i}(t) \tag{17}$$

$$\dot{z}_{4i}(t) = A_2z_{4i}(t) + \bar{C}_{22}z_{2i}(t) + \bar{F}_2f_{s1i}(t) = A_2z_{4i}(t) + v_{2i}(t) \tag{18}$$

where z_{3i} and z_{4i} are the states of filters, and filter matrices A_1 and A_2 are Hurwitz matrices to be designed.

Define $z_{1i}(t) = \begin{bmatrix} z_{1i}(t) \\ z_{3i}(t) \end{bmatrix} \in \mathbb{R}^4$, $z_{2i}(t) = \begin{bmatrix} z_{2i}(t) \\ z_{4i}(t) \end{bmatrix} \in \mathbb{R}^4$. Furthermore, according to (15) and (17), the following augmented system can be obtained:

$$\begin{cases} \dot{z}_{1i}(t) = A_{11}z_{1i}(t) + A_{12}\bar{z}_{2i}(t) + B_{11}u_{0i}(t) + M_{11}\eta_i(t, T^{-1}\bar{z}_i, u_{0i}) + D_{10}d_i(t, T^{-1}\bar{z}_i) \\ v_{1i}(t) = C_1z_{1i}(t) \end{cases} \quad (19)$$

where $A_{11} = \begin{bmatrix} \bar{A}_{11} & \mathbf{0} \\ \bar{C}_{11} & A_1 \end{bmatrix} \in \mathbb{R}^{4 \times 4}$, $A_{12} = \begin{bmatrix} \bar{A}_{12} \\ \mathbf{0} \end{bmatrix} \in \mathbb{R}^{4 \times 3}$, $B_{11} = \begin{bmatrix} \bar{B}_1 \\ \mathbf{0} \end{bmatrix} \in \mathbb{R}^{4 \times 3}$,
 $M_{11} = \begin{bmatrix} \bar{M}_1 \\ \mathbf{0} \end{bmatrix} \in \mathbb{R}^{4 \times 6}$, $D_{10} = \begin{bmatrix} \bar{D}_1 \\ \mathbf{0} \end{bmatrix} \in \mathbb{R}^{4 \times 6}$, $C_1 = \begin{bmatrix} \bar{C}_{11} & \mathbf{0} \\ \mathbf{0} & I \end{bmatrix} \in \mathbb{R}^{2 \times 4}$.

Similarly, based on (16) and (18), there is:

$$\begin{cases} \dot{z}_{2i}(t) = A_{21}z_{2i}(t) + A_{22}\bar{z}_{1i}(t) + B_{21}u_{0i}(t) + M_{21}\eta_i(t, T^{-1}\bar{z}_i, u_{0i}) \\ \quad + D_{20}d_i(t, T^{-1}\bar{z}_i) + E_{21}f_i(t) \\ v_{2i}(t) = C_2z_{2i}(t) \end{cases} \quad (20)$$

where $A_{21} = \begin{bmatrix} \bar{A}_{22} & \mathbf{0} \\ \bar{C}_{22} & A_2 \end{bmatrix} \in \mathbb{R}^{4 \times 4}$, $A_{22} = \begin{bmatrix} \bar{A}_{21} \\ \mathbf{0} \end{bmatrix} \in \mathbb{R}^{4 \times 3}$, $B_{21} = \begin{bmatrix} \bar{B}_2 \\ \mathbf{0} \end{bmatrix} \in \mathbb{R}^{4 \times 3}$,
 $M_{21} = \begin{bmatrix} \bar{M}_2 \\ \mathbf{0} \end{bmatrix} \in \mathbb{R}^{4 \times 6}$, $D_{20} = \begin{bmatrix} \bar{D}_2 \\ \mathbf{0} \end{bmatrix} \in \mathbb{R}^{4 \times 6}$, $E_{21} = \begin{bmatrix} \bar{E}_2 & \mathbf{0} \\ \mathbf{0} & \bar{F}_2 \end{bmatrix} \in \mathbb{R}^{4 \times 2}$, $C_2 = \begin{bmatrix} \bar{C}_{22} & \mathbf{0} \\ \mathbf{0} & I \end{bmatrix} \in \mathbb{R}^{2 \times 4}$, $f_i(t) = \begin{bmatrix} f_{a1i}(t) \\ f_{s1i}(t) \end{bmatrix}$.

Similarly, by using the linear non-singular transformation, the nominal form of system (10) can be transformed into the following two subsystems:

$$\begin{cases} \dot{z}_{1Ni}(t) = A_{11}z_{1Ni}(t) + A_{12}\bar{z}_{2Ni}(t) + B_{11}u_{0Ni}(t) + M_{11}\eta_i(t, T^{-1}\bar{z}_{Ni}, u_{0Ni}) \\ v_{1Ni}(t) = C_1z_{1Ni}(t) \end{cases} \quad (21)$$

$$\begin{cases} \dot{z}_{2Ni}(t) = A_{21}z_{2Ni}(t) + A_{22}\bar{z}_{1Ni}(t) + B_{21}u_{0Ni}(t) + M_{21}\eta_i(t, T^{-1}\bar{z}_{Ni}, u_{0Ni}) \\ v_{2Ni}(t) = C_2z_{2Ni}(t) \end{cases} \quad (22)$$

To sum up, two augmenting subsystems (19) and (20) are obtained after the non-singular transformation of system (9), in which the subsystem formulated in (19) contains disturbances but is free from faults, and the augmenting subsystem (20) is subject to both disturbances and faults. In this way, the actuator and sensor fault in system (9) can be transformed into actuator faults in the augmenting subsystem (20) for research [18].

3.1. Cooperative Unknown Input Observers

Based on the augmented subsystems (19) and (20), cooperative UIOs are designed for multi-UAVs to realize FD and fault estimation in this subsection.

Assumption 3. The disturbance $d_i(t, T^{-1}\bar{z}_i)$ in (19) is bounded and continuously differentiable, so make $\bar{d}_{1i}(t, T^{-1}\bar{z}_i) = D_{10}d_i(t, T^{-1}\bar{z}_i)$; that is, there are positive constants H_{1i} and H_{2i} , such that $|\bar{d}_{1i}(t, T^{-1}\bar{z}_i)| \leq H_{1i}$, $|\dot{\bar{d}}_{1i}(t, T^{-1}\bar{z}_i)| \leq H_{2i}$.

Assumption 4. The fault $f_i(t)$ is bounded, but its upper bound is unknown, so define $\bar{d}_{2i}(t, T^{-1}\bar{z}_i) = D_{20}d_i(t, T^{-1}\bar{z}_i) + E_{21}f_i(t)$, and $\bar{d}_{2i}(t, T^{-1}\bar{z}_i)$ is continuously differentiable; that is, there exists a positive constant H_{3i} , such that $|\dot{\bar{d}}_{2i}(t, T^{-1}\bar{z}_i)| \leq H_{3i}$.

Assumption 5. For the subsystems (19) and (20), there exists a matrix R_i of appropriate dimensions, which satisfies $R_i(t, T^{-1}\bar{z}_i)\dot{\bar{d}}_{1i}(t, T^{-1}\bar{z}_i) = D_{20}d_i(t, T^{-1}\bar{z}_i)$.

Inspired by the work in [36], for the subsystem (19), the proposed cooperative UIOs have the following form:

$$\begin{cases} \dot{\hat{z}}_{1i}(t) = A_{11}\hat{z}_{1i}(t) + A_{12}\hat{z}_{2i}(t) + B_{11}u_{0i}(t) + M_{11}\eta_i(t, T^{-1}\hat{z}_i, u_{0i}) \\ \quad + \hat{d}_{1i}(t, T^{-1}\hat{z}_i) + \zeta_{1i}(\tilde{z}_{1i}(t), \varphi_{1i}(t)) \\ \dot{\hat{d}}_{1i}(t, T^{-1}\hat{z}_i) = \zeta_{2i}(\tilde{z}_{1i}(t), \varphi_{1i}(t)) \end{cases} \quad (23)$$

where $\hat{z}_{1i}(t)$ is the state of observer, $\hat{z}_{2i}(t)$ is the estimation of $\bar{z}_{2i}(t)$, \hat{z}_i is the estimation of \bar{z}_i , $\hat{d}_{1i}(t, T^{-1}\hat{z}_i)$ is the estimation of $\bar{d}_{1i}(t, T^{-1}\bar{z}_i)$, $\varphi_{1i} = \sum_{j \in \Omega_i} a_{ij}(\tilde{z}_{1i}(t) - \tilde{z}_{1j}(t))$, $\tilde{z}_{1i}(t) = z_{1i}(t) - \hat{z}_{1i}(t)$ is the estimation error of $z_{1i}(t)$ of UAV# i , $i = 1, \dots, N$ with total of N follower UAVs. $\zeta_{1i}(\tilde{z}_{1i}(t), \varphi_{1i}(t))$ and $\zeta_{2i}(\tilde{z}_{1i}(t), \varphi_{1i}(t))$ are given as

$$\begin{cases} \zeta_{1i}(\tilde{z}_{1i}(t), \varphi_{1i}(t)) = L_1|\tilde{z}_{1i}(t)|^{a_1}\text{sgn}(\tilde{z}_{1i}(t)) + L_2|\tilde{z}_{1i}(t)|^{b_1+1}\text{sgn}(\tilde{z}_{1i}(t)) \\ \quad + L_1|\varphi_{1i}(t)|^{a_1}\text{sgn}(\varphi_{1i}(t)) + L_2|\varphi_{1i}(t)|^{b_1+1}\text{sgn}(\varphi_{1i}(t)) \\ \zeta_{2i}(\tilde{z}_{1i}(t), \varphi_{1i}(t)) = L_1|\tilde{z}_{1i}(t)|^{a_2}\text{sgn}(\tilde{z}_{1i}(t)) + L_2|\tilde{z}_{1i}(t)|^{b_2+1}\text{sgn}(\tilde{z}_{1i}(t)) \\ \quad + L_1|\varphi_{1i}(t)|^{a_2}\text{sgn}(\varphi_{1i}(t)) + L_2|\varphi_{1i}(t)|^{b_2+1}\text{sgn}(\varphi_{1i}(t)) \end{cases} \quad (24)$$

where L_1, L_2 are positive constants, $0.5 < a_1 < 1, 0.5 < b_1 < 1, a_2 = 2a_1 - 1$, and $b_2 = 2b_1 - 1$ are parameters to be designed, $\text{sgn}(\bullet)$ denotes a sign function.

Then, the following error system is obtained:

$$\begin{cases} \dot{\tilde{z}}_{1i}(t) = A_{11}\tilde{z}_{1i}(t) + A_{12}\tilde{z}_{2i}(t) + M_{11}\tilde{\eta}_i(t, T^{-1}\tilde{z}_i, u_{0i}) + \tilde{d}_{1i}(t, T^{-1}\tilde{z}_i) - \zeta_{1i}(\tilde{z}_{1i}(t), \varphi_{1i}(t)) \\ \dot{\tilde{d}}_{1i}(t) = \tilde{d}_{1i}(t) - \zeta_{2i}(\tilde{z}_{1i}(t), \varphi_{1i}(t)) \end{cases} \quad (25)$$

where $\tilde{d}_{1i}(t, T^{-1}\tilde{z}_i) = \bar{d}_{1i}(t, T^{-1}\bar{z}_i) - \hat{d}_{1i}(t, T^{-1}\hat{z}_i)$ is the estimation error of $\bar{d}_{1i}(t, T^{-1}\bar{z}_i)$, $\tilde{\eta}_i(t, T^{-1}\tilde{z}_i, u_{0i}) = \eta_i(t, T^{-1}\bar{z}_i, u_{0i}) - \eta_i(t, T^{-1}\hat{z}_i, u_{0i})$ is the estimation of $\eta_i(t, T^{-1}\bar{z}_i, u_{0i})$, $\tilde{z}_{2i}(t) = \bar{z}_{2i}(t) - \hat{z}_{2i}(t)$ is the estimation error of $\bar{z}_{2i}(t)$.

Similarly, according to the subsystem (20), the cooperative UIOs are designed as:

$$\begin{cases} \dot{\hat{z}}_{2i}(t) = A_{21}\hat{z}_{2i}(t) + A_{22}\bar{z}_{1i}(t) + B_{21}u_{0i}(t) + M_{21}\eta_i(t, T^{-1}\hat{z}_i, u_{0i}) \\ \quad + \hat{d}_{2i}(t, T^{-1}\hat{z}_i) + (\hat{L} + \delta)\zeta_{3i}(\tilde{z}_{5i}(t), \varphi_{2i}(t)) \\ \dot{\hat{d}}_{2i}(t, T^{-1}\hat{z}_i) = \zeta_{4i}(\tilde{z}_{5i}(t), \varphi_{2i}(t)) \end{cases} \quad (26)$$

where $\hat{z}_{2i}(t)$ is the state of observer, $\hat{d}_{2i}(t, T^{-1}\hat{z}_i)$ is the estimation of $\bar{d}_{2i}(t, T^{-1}\bar{z}_i)$,

$$\tilde{z}_{5i}(t) = \begin{bmatrix} v_{2i1}(t) - \hat{v}_{2i1}(t) \\ z_{2i2}(t) - \hat{z}_{2i2}(t) \\ z_{2i3}(t) - \hat{z}_{2i3}(t) \\ v_{2i2}(t) - \hat{v}_{2i2}(t) \end{bmatrix}, \hat{v}_{2i}(t) = \begin{bmatrix} \hat{v}_{2i1} \\ \hat{v}_{2i2} \end{bmatrix} = C_2\hat{z}_{2i}(t), \varphi_{2i} = \sum_{j \in \Omega_i} a_{ij}(\tilde{z}_{5i} - \tilde{z}_{5j}).$$

$\zeta_{3i}(\tilde{z}_{5i}(t), \varphi_{2i}(t))$ and $\zeta_{4i}(\tilde{z}_{5i}(t), \varphi_{2i}(t))$ are given by

$$\begin{cases} \zeta_{3i}(\tilde{z}_{5i}(t), \varphi_{2i}(t)) = L_3|\tilde{z}_{5i}(t)|^{a_3}\text{sgn}(\tilde{z}_{5i}(t)) + L_4|\tilde{z}_{5i}(t)|^{b_3+1}\text{sgn}(\tilde{z}_{5i}(t)) \\ \quad + L_3|\varphi_{2i}(t)|^{a_3}\text{sgn}(\varphi_{2i}(t)) + L_4|\varphi_{2i}(t)|^{b_3+1}\text{sgn}(\varphi_{2i}(t)) \\ \zeta_{4i}(\tilde{z}_{5i}(t), \varphi_{2i}(t)) = L_3|\tilde{z}_{5i}(t)|^{a_4}\text{sgn}(\tilde{z}_{5i}(t)) + L_4|\tilde{z}_{5i}(t)|^{b_4+1}\text{sgn}(\tilde{z}_{5i}(t)) \\ \quad + L_3|\varphi_{2i}(t)|^{a_4}\text{sgn}(\varphi_{2i}(t)) + L_4|\varphi_{2i}(t)|^{b_4+1}\text{sgn}(\varphi_{2i}(t)) \end{cases} \quad (27)$$

where L_3, L_4 are positive constants, $0.5 < a_3 < 1, 0.5 < b_3 < 1, a_4 = 2a_3 - 1$, and $b_4 = 2b_3 - 1$ are designed parameters. δ is a small constant. Suppose the upper bound of

$\bar{d}_{2i}(t, T^{-1}\bar{z}_i)$ is L , which is unknown. \hat{L} is the estimation of L , and its adaptive law is designed as

$$\dot{\hat{L}} = L_3 P_2 |\bar{z}_{5i}(t)|^{a_3+1} + L_4 P_2 |\bar{z}_{5i}(t)|^{b_3+2} + L_3 P_2 |\varphi_{2i}(t)|^{a_3+1} + L_4 P_2 |\varphi_{2i}(t)|^{b_3+2} \tag{28}$$

where P_2 is a stable matrix to be designed.

Further, the following error system is obtained:

$$\begin{cases} \dot{\bar{z}}_{2i}(t) = A_{21}\bar{z}_{2i}(t) + M_{21}\tilde{\eta}_i(t, T^{-1}\bar{z}_i, u_{0i}) + \tilde{d}_{2i}(t, T^{-1}\bar{z}_i) - (\hat{L} + \delta)\zeta_{3i}(\bar{z}_{5i}(t), \varphi_{2i}(t)) \\ \dot{\tilde{d}}_{2i}(t, T^{-1}\bar{z}_i) = \dot{\hat{d}}_{2i}(t, T^{-1}\hat{z}_i) - \zeta_{4i}(\bar{z}_{5i}(t), \varphi_{2i}(t)) \end{cases} \tag{29}$$

where $\bar{z}_{2i}(t) = z_{2i}(t) - \hat{z}_{2i}(t)$ is the estimation error of $z_{2i}(t)$, $\tilde{d}_{2i}(t, T^{-1}\bar{z}_i) = \bar{d}_{2i}(t, T^{-1}\bar{z}_i) - \hat{d}_{2i}(t, T^{-1}\hat{z}_i)$ is the estimation error of $\bar{d}_{2i}(t, T^{-1}\bar{z}_i)$.

Theorem 1. *The designed cooperative UIOs in the form of (23) and (26) can guarantee that the estimation errors are asymptotically stable, if there exist positive definite matrices P_1 and P_2 , such that the following linear matrix inequality (LMI) is satisfied.*

$$Q = \begin{bmatrix} \frac{I}{2} \otimes (P_1 A_{11} + A_{11}^T P_1 + P_1) & \frac{I}{2} \otimes P_1 \check{A}_{12} & \frac{I}{2} \otimes P_1 & * \\ \frac{I}{2} \otimes P_1 \check{A}_{12} & \frac{I}{2} \otimes \left(P_2 A_{21} + A_{21}^T P_2 + 2L_p \|\bar{M}_{21}\| \|T^{-1}\| P_2 \right) & * & \frac{I}{2} \otimes P_2 \\ \frac{I}{2} \otimes P_1^T & * & \frac{3}{2} I & * \\ * & \frac{I}{2} \otimes P_2^T & * & \frac{3}{2} I \end{bmatrix} < 0 \tag{30}$$

Proof. Define the vectors as $\bar{z}_1 = [z_{11}^T, z_{12}^T, \dots, z_{1N}^T]^T$, $\bar{z}_2 = [z_{21}^T, z_{22}^T, \dots, z_{2N}^T]^T$, $\tilde{d}_1 = [d_{11}^T, d_{12}^T, \dots, d_{1N}^T]^T$, $\tilde{d}_2 = [d_{21}^T, d_{22}^T, \dots, d_{2N}^T]^T$, $\bar{z}_5 = [z_{51}^T, z_{52}^T, \dots, z_{5N}^T]^T$, select a Lyapunov function as:

$$V = V_1 + V_2 \tag{31}$$

where $V_1 = \frac{1}{2} \bar{z}_1^T (I \otimes P_1) \bar{z}_1 + \frac{1}{2} \tilde{d}_1^T \tilde{d}_1$, $V_2 = \frac{1}{2} \bar{z}_2^T (I \otimes P_2) \bar{z}_2 + \frac{1}{2} \tilde{d}_2^T \tilde{d}_2 + \frac{1}{2} \check{L}^T \check{L}$. \otimes represents the Kronecker product.

By considering (25), differentiating V_1 yields:

$$\begin{aligned} \dot{V}_1 = & \frac{1}{2} \bar{z}_1^T \left[I \otimes (P_1 A_{11} + A_{11}^T P_1) \right] \bar{z}_1 + \bar{z}_1^T (I \otimes P_1 A_{12}) \bar{z}_2 + \bar{z}_1^T (I \otimes P_1 M_{11}) \tilde{\eta} + \bar{z}_1^T (I \otimes P_1) \tilde{d}_1 \\ & - \bar{z}_1^T (\mathcal{L} + I) \otimes P_1 L_1 |\bar{z}_1|^{a_1} \text{sgn}(\bar{z}_1) - \bar{z}_1^T (\mathcal{L} + I) \otimes P_1 L_2 |\bar{z}_1|^{b_1+1} \text{sgn}(\bar{z}_1) \\ & + \tilde{d}_1^T \dot{\tilde{d}}_1 - \tilde{d}_1^T (\mathcal{L} + I) \otimes L_1 |\bar{z}_1|^{a_2} \text{sgn}(\bar{z}_1) - \tilde{d}_1^T (\mathcal{L} + I) \otimes L_2 |\bar{z}_1|^{b_2+1} \text{sgn}(\bar{z}_1) \end{aligned} \tag{32}$$

Note that:

$$\begin{aligned} \|\tilde{\eta}_i(t, T^{-1}\bar{z}_i, u_{0i})\| &= \left\| \tilde{\eta}_i \left(t, T^{-1} \begin{bmatrix} \mathbf{0} \\ \bar{z}_{2i} \end{bmatrix}, u_{0i} \right) \right\| \\ &\leq L_p \|T^{-1}\| \|\bar{z}_{2i}\| \\ &\leq L_p \|T^{-1}\| \|\bar{z}_{2i}\| \end{aligned} \tag{33}$$

Based on (33), Assumption 2, and Young’s inequality, it is shown that:

$$\begin{aligned} \tilde{z}_1^T(I \otimes P_1 M_{11}) \tilde{\eta}(t, T^{-1} \tilde{z}, u_0) &= \tilde{z}_1^T(I \otimes P_1 M_{11}) \tilde{\eta}\left(t, T^{-1} \begin{bmatrix} \mathbf{0} \\ \tilde{z}_2 \end{bmatrix}, u_0\right) \\ &\leq L_p \tilde{z}_1^T(I \otimes P_1 \check{M}_{11}) \left\| T^{-1} \right\| \tilde{z}_2 \\ &\leq L_p \tilde{z}_1^T(I \otimes P_1 \bar{M}_{11}) \left\| T^{-1} \right\| \tilde{z}_2 \\ &\leq \frac{1}{2} \tilde{z}_1^T P_1 \tilde{z}_1 + \frac{1}{2} L_p^2 \|\bar{M}_{11}\|^2 \left\| T^{-1} \right\|^2 \tilde{z}_2^T (I \otimes P_1^{-1}) \tilde{z}_2 \end{aligned} \tag{34}$$

where $\check{M}_{11} \in \mathbb{R}^{4 \times 3}$, $\bar{M}_{11} = [\check{M}_{11} \mathbf{0}] \in \mathbb{R}^{4 \times 4}$.

According to (32), (34) and using Young’s inequality, the following inequality can be obtained:

$$\begin{aligned} \dot{V}_1 &\leq \frac{1}{2} \tilde{z}_1^T \left[I \otimes (P_1 A_{11} + A_{11}^T P_1 + P_1) \right] \tilde{z}_1 + \tilde{z}_1^T (I \otimes P_1 \check{A}_{12}) \tilde{z}_2 + \tilde{z}_1^T (I \otimes P_1) \check{d}_1 + \frac{3}{2} \check{d}_1^T \check{d}_1 \\ &\quad + \frac{1}{2} L_p^2 \|\bar{M}_{11}\|^2 \left\| T^{-1} \right\|^2 \tilde{z}_2^T (I \otimes P_1^{-1}) \tilde{z}_2 - (\mathcal{L} + I) \otimes P_1 \left(L_1 |\tilde{z}_1(t)|^{a_1+1} + L_2 |\tilde{z}_1(t)|^{b_1+2} \right) \\ &\quad + \frac{1}{2} \check{d}_1^T \check{d}_1 + \frac{1}{2} (\mathcal{L} + I) \left(L_1 |\tilde{z}_1(t)|^{2a_2} + L_2 |\tilde{z}_1(t)|^{2b_2+2} \right) \end{aligned} \tag{35}$$

where $\check{A}_{12} = [A_{12} \mathbf{0}] \in \mathbb{R}^{4 \times 4}$.

By considering (29) and differentiating V_2 , one has:

$$\begin{aligned} \dot{V}_2 &= \frac{1}{2} \tilde{z}_2^T \left[I \otimes (P_2 A_{21} + A_{21}^T P_2) \right] \tilde{z}_2 + \tilde{z}_2^T (I \otimes P_2 M_{21}) \tilde{\eta} + \tilde{z}_2^T (I \otimes P_2) \check{d}_2 \\ &\quad - \tilde{z}_2^T [(\mathcal{L} + I) \otimes P_2 (\hat{L} + \delta)] \left(L_3 |\tilde{z}_5|^{a_3} \text{sgn}(\tilde{z}_5) + L_4 |\tilde{z}_5|^{b_3+1} \text{sgn}(\tilde{z}_5) \right) \\ &\quad + \check{d}_2^T \check{d}_2 - \check{d}_2^T (\mathcal{L} + I) \otimes L_3 |\tilde{z}_5|^{a_4} \text{sgn}(\tilde{z}_5) - \check{d}_2^T (\mathcal{L} + I) \otimes L_4 |\tilde{z}_5|^{b_4+1} \text{sgn}(\tilde{z}_5) \\ &\quad + \check{L}^T \check{L} - (L - \hat{L}) \left[(\mathcal{L} + I) \otimes P_2 L_3 |\tilde{z}_5|^{a_3+1} + (\mathcal{L} + I) \otimes P_2 L_3 |\tilde{z}_5|^{b_3+2} \right] \end{aligned} \tag{36}$$

Similarly, notice that:

$$\begin{aligned} \tilde{z}_2^T (I \otimes P_2 M_{21}) \tilde{\eta}(t, T^{-1} \tilde{z}, u_0) &= \tilde{z}_2^T (I \otimes P_2 M_{21}) \tilde{\eta}\left(t, T^{-1} \begin{bmatrix} \mathbf{0} \\ \tilde{z}_2 \end{bmatrix}, u_0\right) \\ &\leq L_p \tilde{z}_2^T (I \otimes P_2 \check{M}_{21}) \left\| T^{-1} \right\| \tilde{z}_2 \\ &\leq L_p \tilde{z}_2^T (I \otimes P_2) \|\bar{M}_{21}\| \left\| T^{-1} \right\| \tilde{z}_2 \end{aligned} \tag{37}$$

where $\check{M}_{21} \in \mathbb{R}^{4 \times 3}$, $\bar{M}_{21} = [\check{M}_{21} \mathbf{0}] \in \mathbb{R}^{4 \times 4}$.

According to (36), (37), and using Young’s inequality, the following inequality can be obtained.

$$\begin{aligned} \dot{V}_2 &\leq \frac{1}{2} \tilde{z}_2^T \left[I \otimes (P_2 A_{21} + A_{21}^T P_2 + 2L_p \|\bar{M}_{21}\| \left\| T^{-1} \right\| P_2) \right] \tilde{z}_2 + \tilde{z}_2^T (I \otimes P_2) \check{d}_2 + \frac{3}{2} \check{d}_2^T \check{d}_2 \\ &\quad - [(\mathcal{L} + I) \otimes P_2 \delta] \left(L_3 |\tilde{z}_5(t)|^{a_3+1} + L_4 |\tilde{z}_5(t)|^{b_3+2} \right) + \frac{1}{2} \check{d}_2^T \check{d}_2 + \frac{1}{2} \check{L}^T \check{L} + \frac{1}{2} \check{L}^T \check{L} \\ &\quad - [(\mathcal{L} + I) \otimes P_2 L] \left(L_3 |\tilde{z}_5(t)|^{a_3+1} + L_4 |\tilde{z}_5(t)|^{b_3+2} \right) \\ &\quad + \frac{1}{2} (\mathcal{L} + I) \left(L_3 |\tilde{z}_5(t)|^{2a_4} + L_4 |\tilde{z}_5(t)|^{2b_4+2} \right) \end{aligned} \tag{38}$$

Define $\check{e} = [\tilde{z}_1^T, \tilde{z}_2^T, \check{d}_1^T, \check{d}_2^T]^T$, then, one obtains

$$\begin{aligned}
 \dot{V} &= \dot{V}_1 + \dot{V}_2 \\
 &\leq \frac{1}{2} \tilde{z}_1^T \left[\mathbf{I} \otimes \left(\mathbf{P}_1 \mathbf{A}_{11} + \mathbf{A}_{11}^T \mathbf{P}_1 + \mathbf{P}_1 \right) \right] \tilde{z}_1 + \tilde{z}_1^T \left(\mathbf{I} \otimes \mathbf{P}_1 \check{\mathbf{A}}_{12} \right) \tilde{z}_2 + \tilde{z}_1^T \left(\mathbf{I} \otimes \mathbf{P}_1 \right) \check{\mathbf{d}}_1 + \tilde{z}_2^T \left(\mathbf{I} \otimes \mathbf{P}_2 \right) \check{\mathbf{d}}_2 \\
 &\quad + \frac{1}{2} \tilde{z}_2^T \left[\mathbf{I} \otimes \left(\mathbf{P}_2 \mathbf{A}_{21} + \mathbf{A}_{21}^T \mathbf{P}_2 + 2L_p \|\check{\mathbf{M}}_{21}\| \left\| \mathbf{T}^{-1} \right\| \left\| \mathbf{P}_2 + L_p^2 \|\check{\mathbf{M}}_{11}\|^2 \left\| \mathbf{T}^{-1} \right\|^2 \mathbf{P}_1^{-1} \right) \right] \tilde{z}_2 \\
 &\quad - (\mathcal{L} + \mathbf{I}) \otimes \mathbf{P}_1 \left(L_1 |\tilde{z}_1(t)|^{a_1+1} + L_2 |\tilde{z}_1(t)|^{b_1+2} \right) + \frac{3}{2} \check{\mathbf{d}}_1^T \check{\mathbf{d}}_1 + \frac{3}{2} \check{\mathbf{d}}_2^T \check{\mathbf{d}}_2 \\
 &\quad - [(\mathcal{L} + \mathbf{I}) \otimes \mathbf{P}_2 \delta] \left(L_3 |\tilde{z}_5(t)|^{a_3+1} + L_4 |\tilde{z}_5(t)|^{b_3+2} \right) \\
 &\quad + \frac{1}{2} (\mathcal{L} + \mathbf{I}) \left(L_1 |\tilde{z}_1(t)|^{2a_2} + L_2 |\tilde{z}_1(t)|^{2b_2+2} \right) + \frac{1}{2} (\mathcal{L} + \mathbf{I}) \left(L_3 |\tilde{z}_5(t)|^{2a_4} + L_4 |\tilde{z}_5(t)|^{2b_4+2} \right) \tag{39} \\
 &\quad + \frac{1}{2} \dot{\check{\mathbf{d}}}_1^T \check{\mathbf{d}}_1 + \frac{1}{2} \dot{\check{\mathbf{d}}}_2^T \check{\mathbf{d}}_2 + \frac{1}{2} \check{\mathbf{L}}^T \check{\mathbf{L}} + \frac{1}{2} \dot{\check{\mathbf{L}}}^T \check{\mathbf{L}} - [(\mathcal{L} + \mathbf{I}) \otimes \mathbf{P}_2 \mathbf{L}] \left(L_3 |\tilde{z}_5(t)|^{a_3+1} + L_4 |\tilde{z}_5(t)|^{b_3+2} \right) \\
 &\leq \tilde{\mathbf{e}}^T \mathbf{Q} \tilde{\mathbf{e}} - (\mathcal{L} + \mathbf{I}) \otimes \mathbf{P}_1 \left(L_1 |\tilde{z}_1(t)|^{a_1+1} + L_2 |\tilde{z}_1(t)|^{b_1+2} \right) \\
 &\quad - [(\mathcal{L} + \mathbf{I}) \otimes \mathbf{P}_2 \delta] \left(L_3 |\tilde{z}_5(t)|^{a_3+1} + L_4 |\tilde{z}_5(t)|^{b_3+2} \right) \\
 &\quad + \frac{1}{2} (\mathcal{L} + \mathbf{I}) \left(L_1 |\tilde{z}_1(t)|^{2a_2} + L_2 |\tilde{z}_1(t)|^{2b_2+2} \right) + \frac{1}{2} (\mathcal{L} + \mathbf{I}) \left(L_3 |\tilde{z}_5(t)|^{2a_4} + L_4 |\tilde{z}_5(t)|^{2b_4+2} \right) \\
 &\quad + \frac{1}{2} \dot{\check{\mathbf{d}}}_1^T \check{\mathbf{d}}_1 + \frac{1}{2} \dot{\check{\mathbf{d}}}_2^T \check{\mathbf{d}}_2 + \frac{1}{2} \check{\mathbf{L}}^T \check{\mathbf{L}} + \frac{1}{2} \dot{\check{\mathbf{L}}}^T \check{\mathbf{L}} - [(\mathcal{L} + \mathbf{I}) \otimes \mathbf{P}_2 \mathbf{L}] \left(L_3 |\tilde{z}_5(t)|^{a_3+1} + L_4 |\tilde{z}_5(t)|^{b_3+2} \right)
 \end{aligned}$$

Thus, according to the Lyapunov stability theorem, if $\mathbf{Q} < 0$, the estimation errors are asymptotically stable and can converge to zero.

This ends the proof. \square

3.2. Fault Detection and Estimation

Considering the influence of disturbances on FD and fault estimation in the augmented subsystem (20), time-varying adaptive thresholds were designed to detect faults in the system. Combined with the estimation of the disturbances from the cooperative UIOs (23), the adaptive thresholds proposed were the following:

$$\begin{cases} \varrho_{1i} = \mathbf{C}_{2i} \hat{\mathbf{R}}_i \left(t, \mathbf{T}^{-1} \hat{\mathbf{z}}_i \right) \hat{\mathbf{d}}_{1i} \left(t, \mathbf{T}^{-1} \hat{\mathbf{z}}_i \right) + \sigma_i \\ \varrho_{2i} = \mathbf{C}_{2i} \hat{\mathbf{R}}_i \left(t, \mathbf{T}^{-1} \hat{\mathbf{z}}_i \right) \hat{\mathbf{d}}_{1i} \left(t, \mathbf{T}^{-1} \hat{\mathbf{z}}_i \right) - \sigma_i \end{cases} \tag{40}$$

where ϱ_{1i} and ϱ_{2i} are the upper and lower bounds of the thresholds, respectively. $\varrho_{1i} = [\varrho_{1i1}, \varrho_{1i2}]^T$, $\varrho_{2i} = [\varrho_{2i1}, \varrho_{2i2}]^T$, $\sigma_i = [\sigma_{i1}, \sigma_{i2}]^T$. σ_{i1} and σ_{i2} are the offset of the adaptive thresholds, where $\sigma_{i1} = H_{1i}/9$, $\sigma_{i2} = H_{1i}/3$. $\hat{\mathbf{R}}_i \left(t, \mathbf{T}^{-1} \hat{\mathbf{z}}_i \right)$ is given as

$$\hat{\mathbf{R}}_i \left(t, \mathbf{T}^{-1} \hat{\mathbf{z}}_i \right) = \begin{bmatrix} -\cos \gamma_i \cos \chi_i & -\cos \gamma_i \sin \chi_i & -\sin \gamma_i & 0 \\ \sin \chi_i / \hat{V}_i \cos \gamma_i & -\cos \chi_i / \hat{V}_i \cos \gamma_i & 0 & 0 \\ \sin \gamma_i \cos \chi_i / \hat{V}_i & \sin \gamma_i \sin \chi_i / \hat{V}_i & -\cos \gamma_i / \hat{V}_i & 0 \\ 0 & 0 & 0 & 0 \end{bmatrix}$$

According to the subsystems (20), (22), and the designed UIO (26), there is

$$\mathbf{z}_{2Ni}(t) = \hat{\mathbf{z}}_{2i}(t) - \hat{\mathbf{d}}_{2i} \left(t, \mathbf{T}^{-1} \hat{\mathbf{z}}_i \right) \tag{41}$$

A set of residual signals can be calculated as $\mathbf{r}_i = \mathbf{v}_{2i}(t) - \mathbf{C}_{2i} \mathbf{z}_{Ni}(t)$. Then, the following FD conditions are given as follow:

$$\begin{cases} \varrho_{2i} < \mathbf{r}_i < \varrho_{1i}, & \text{no fault} \\ \mathbf{r}_i \leq \varrho_{2i} \text{ or } \mathbf{r}_i \geq \varrho_{1i}, & \text{fault alarm} \end{cases} \tag{42}$$

where $r_i = [r_{i1}, r_{i2}]^T$. In combination with the subsystem (20), it can be seen that the residuals r_{i1} and r_{i2} were caused by actuator fault and sensor fault, respectively. Therefore, the actuator fault and sensor fault in the system could be detected, respectively.

For ease of analysis, define $\bar{d}_i = Dd_i(t)$. According to Theorem 1, the estimation of the disturbances in system (19) \hat{d}_{1i} converge to \bar{d}_{1i} as the observation errors in (25) converge to zero. Further, the estimation of disturbances in system (20) can be expressed as $D_{20}\hat{d}_i = \hat{R}_i\hat{d}_{1i}$. Thus, $\hat{d}_{1i} = \begin{bmatrix} D_1\hat{d}_i \\ \mathbf{0} \end{bmatrix}$, $\hat{R}_i\hat{d}_{1i} = \begin{bmatrix} D_2\hat{d}_i \\ \mathbf{0} \end{bmatrix}$ can be obtained. Then, the estimation of disturbances in the original system can be expressed as $\hat{d}_i = T^{-1} \begin{bmatrix} \bar{D}_1\hat{d}_i \\ \bar{D}_2\hat{d}_i \end{bmatrix} = \begin{bmatrix} \hat{W}_i \\ \hat{W}_i \end{bmatrix}$.

Similarly, according to the system (9), define $\bar{f}_{ai} = Ef_{ai}$, $\bar{f}_{si} = Ff_{si}$. According to Theorem 1, the estimation of the disturbances in system (20) \hat{d}_{2i} converge to \bar{d}_{2i} . Further, the estimation of disturbances in system (20) can be expressed as $\hat{d}_{2i} = D_{20}\hat{d}_i + E_{21}\hat{f}_i$. Thus, it can be obtained that $E_{21}\hat{f}_i = \hat{d}_{2i} - R_i\hat{d}_{1i}$. Let $E_{21}\hat{f}_i = \begin{bmatrix} \hat{f}_{1i} \\ \hat{f}_{2i} \end{bmatrix}$. According to (13), the estimation of faults in the original system can be expressed as:

$$\begin{cases} \hat{f}_{ai} = T^{-1} \begin{bmatrix} \mathbf{0}_{3 \times 1} \\ \hat{f}_{1i} \end{bmatrix} \\ \hat{f}_{si} = S^{-1} \begin{bmatrix} 0 \\ \hat{f}_{2i} \end{bmatrix} \end{cases} \tag{43}$$

4. Fault-Tolerant Cooperative Control Scheme Design

Considering state constraint, a fixed-time FTCC law is designed, based on backstepping control, in this subsection.

Define $x_{10} = [x_0, y_0, z_0]^T$ as the position vector of the leader. Define $x_{1i} = [x_i, y_i, z_i]^T$ as the position vector of the follower UAV# i , $i = 1, 2, \dots, N$. The expected relative position between UAVs is defined as $R_{ij} \in R^3, i, j \in 0, 1, \dots, N$. Thus, the cooperative formation position error is defined as:

$$r_{ij} = x_{1i} - x_{1j} - R_{ij}, i, j \in 0, 1, 2, \dots, N \tag{44}$$

Further, by taking the communication network into account, the generalized position tracking error of the i th UAV is given as:

$$e_{1i} = \frac{1}{\Gamma_i} \sum_{j \in \Omega_i} a_{ij}r_{ij} = x_{1i} - \frac{1}{\Gamma_i} \sum_{j \in \Omega_i} a_{ij}(x_{1j} + R_{ij}) \tag{45}$$

where $i = 1, 2, \dots, N, j = 0, 1, 2, \dots, N$. $\Gamma_i = \sum_{j \in \Omega_i} a_{ij}$, Ω_i represents the neighbor set of the i th UAV. Then, let $x_{1di} = \frac{1}{\Gamma_i} \sum_{j \in \Omega_i} (x_{1j} + R_{ij})$.

The state transformation with scaling function is proposed to keep the state variables within corresponding constraints. Define:

$$X_{2ih} = \frac{x_{2ih}}{(\underline{x}_{2ih} + \hat{x}_{2ih})(\bar{x}_{2ih} - \hat{x}_{2ih})} \tag{46}$$

where $h = 1, 2, 3$. \hat{x}_{2ih} is the estimation of x_{2ih} , \underline{x}_{2ih} is the absolute value of lower bound of x_{2ih} , \bar{x}_{2ih} is the absolute value of upper bound of x_{2ih} . Then, the constraint of x_{2ih} can be ensured, while the boundedness of X_{2ih} is ensured. Thus, state x_{2ih} satisfied $-\underline{x}_{2ih} < x_{2ih} < \bar{x}_{2ih}$ if its initial condition satisfying $-\underline{x}_{2ih} < x_{2ih}(0) < \bar{x}_{2ih}$.

Taking the derivative of X_{2ih} provides:

$$\dot{X}_{2ih} = \eta_{ih}\dot{x}_{2ih} + \zeta_{ih} \tag{47}$$

where $X_{2i} = [X_{2i1}, X_{2i2}, X_{2i3}]^T$, $\eta_{ih} = 1 / (\underline{x}_{2ih} + \hat{x}_{2ih})(\bar{x}_{2ih} - \hat{x}_{2ih})$, $\boldsymbol{\eta}_i = \text{diag}\{\eta_{i1}, \eta_{i2}, \eta_{i3}\}$, $\zeta_{ih} = (\underline{x}_{2ih} - \bar{x}_{2ih} + 2\hat{x}_{2ih})\hat{x}_{2ih}x_{2ih} / (\underline{x}_{2ih} + \hat{x}_{2ih})^2(\bar{x}_{2ih} - \hat{x}_{2ih})^2$, $\boldsymbol{\zeta}_i = [\zeta_{i1}, \zeta_{i2}, \zeta_{i3}]^T$.

Choose the TBLF as:

$$V_{c1i} = \frac{k_b^2}{\pi} \sum_{h=1}^3 \tan\left(\frac{\pi e_{1ih}^2}{2k_b^2}\right) \tag{48}$$

where k_b is a constant. Then, the position tracking error e_{1ih} , $h = 1, 2, 3$, can be limited and satisfies $|e_{1ih}| < k_b$ if $|e_{1ih}| < k_b$ holds.

By differentiating (48), one yields:

$$\begin{aligned} \dot{V}_{c1i} &= \mathbf{e}_{1i}^T \mathbf{A}_{1i} \dot{\mathbf{e}}_{1i} \\ &= \mathbf{e}_{1i}^T \mathbf{A}_{1i} (\dot{\mathbf{x}}_{1i} - \dot{\mathbf{x}}_{1di}) \\ &= \mathbf{e}_{1i}^T \mathbf{A}_{1i} (\mathbf{F}_{1i} + \mathbf{G}_{1i}(\check{\mathbf{x}}_{2i} - \mathbf{f}_{si}) + \mathbf{W}_i - \dot{\mathbf{x}}_{1di}) \\ &= \mathbf{e}_{1i}^T \mathbf{A}_{1i} (\mathbf{F}_{1i} + \mathbf{G}_{1i} \mathbf{K}_{1i} \mathbf{X}_{2i} + \mathbf{W}_i - \dot{\mathbf{x}}_{1di}) \\ &= \mathbf{e}_{1i}^T \mathbf{A}_{1i} (\mathbf{F}_{1i} + \mathbf{G}_{1i} \mathbf{K}_{1i} (\mathbf{E}_{2i} + \mathbf{X}_{2di}) + \mathbf{W}_i - \dot{\mathbf{x}}_{1di}) \end{aligned} \tag{49}$$

where $\mathbf{A}_{1i} = \text{diag}\{A_{1i1}, A_{1i2}, A_{1i3}\}$, $A_{1ih} = 1 / \cos^2(\pi e_{1ih}^2 / 2k_b^2)$, $h = 1, 2, 3$.

$\mathbf{K}_{1i} = \text{diag}\{(\underline{x}_{2i1} + \hat{x}_{2i1})(\bar{x}_{2i1} - \hat{x}_{2i1}), (\underline{x}_{2i2} + \hat{x}_{2i2})(\bar{x}_{2i2} - \hat{x}_{2i2}), (\underline{x}_{2i3} + \hat{x}_{2i3})(\bar{x}_{2i3} - \hat{x}_{2i3})\}$.

$\mathbf{E}_{2i} = \mathbf{X}_{2i} - \mathbf{X}_{2di}$, \mathbf{X}_{2di} is the virtual control signal to be designed.

Then, based on (49), the virtual control signal is designed as:

$$\mathbf{X}_{2di} = \mathbf{G}_{1i}^{-1} \mathbf{K}_{1i}^{-1} \left[-\hat{\mathbf{F}}_{1i} + \dot{\mathbf{x}}_{1di} - \hat{\mathbf{W}}_i - \mathbf{A}_{1i}^{-1} \left(\mathbf{K}_{2i} \text{sig}^{2p_i-1}(\mathbf{e}_{1i}) + \mathbf{K}_{3i} \text{sig}^{2q_i-1}(\mathbf{e}_{1i}) + \frac{3}{2} \mathbf{A}_{1i}^2 \mathbf{e}_{1i} \right) \right] \tag{50}$$

where $\hat{\mathbf{F}}_{1i}$ is the estimation of \mathbf{F}_{1i} , which contains the estimation of state variables. $\hat{\mathbf{W}}_i$ is the estimation of \mathbf{W}_i . $\mathbf{K}_{2i} = \text{diag}\{K_{2i1}, K_{2i2}, K_{2i3}\}$ and $\mathbf{K}_{3i} = \text{diag}\{K_{3i1}, K_{3i2}, K_{3i3}\}$ are designed parameter matrices, $K_{2i1}, K_{2i2}, K_{2i3}, K_{3i1}, K_{3i2}, K_{3i3} > 0$. p_i, q_i are designed parameters, which satisfies $0.5 < p_i < 1, q_i > 1$. $\text{sig}^a(\bullet) = |\bullet|^a \text{sgn}(\bullet)$.

Define $\check{X}_{2ih} = \check{x}_{2ih} / (\underline{x}_{2ih} + \hat{x}_{2ih})(\bar{x}_{2ih} - \hat{x}_{2ih})$, $h = 1, 2, 3$. $\check{\mathbf{X}}_{2i} = [\check{X}_{2i1}, \check{X}_{2i2}, \check{X}_{2i3}]^T$. Furthermore, considering the introduced sensor fault (6), the desired reference of $\check{\mathbf{X}}_{2i}$ is developed as:

$$\check{\mathbf{X}}_{2ci} = \mathbf{G}_{1i}^{-1} \mathbf{K}_{1i}^{-1} \left[-\hat{\mathbf{F}}_{1i} + \dot{\mathbf{x}}_{1di} - \hat{\mathbf{W}}_i - \mathbf{A}_{1i}^{-1} \left(\mathbf{K}_{2i} \text{sig}^{2p_i-1}(\mathbf{e}_{1i}) + \mathbf{K}_{3i} \text{sig}^{2q_i-1}(\mathbf{e}_{1i}) + \frac{3}{2} \mathbf{A}_{1i}^2 \mathbf{e}_{1i} \right) \right] + \mathbf{K}_{1i}^{-1} \hat{\mathbf{f}}_{si} \tag{51}$$

where $\hat{\mathbf{f}}_{si} = [\hat{f}_{si2}, 0, 0]^T$ is the estimation of the sensor fault.

A new variable $\check{\mathbf{X}}_{2di}$ is introduced to avoid direct differentiation of $\check{\mathbf{X}}_{2ci}$ by using dynamic surface control [41]. Then, a nonlinear filter is proposed as follows:

$$\dot{\check{\mathbf{X}}}_{2di} = -\boldsymbol{\eta}_{2i} \left(\text{sig}^{s_{1i}-1}(\check{\mathbf{E}}_{2i}) + \text{sig}^{s_{2i}-1}(\check{\mathbf{E}}_{2i}) \right) - \frac{1}{2} \check{\mathbf{E}}_{2i} \tag{52}$$

where $\boldsymbol{\eta}_{2i} = \text{diag}\{\eta_{2i1}, \eta_{2i2}, \eta_{2i3}\}$ is a designed parameter matrix, $\eta_{2i1}, \eta_{2i2}, \eta_{2i3} > 0$. s_{1i}, s_{2i} are positive constants.

Define $\check{\check{\mathbf{E}}}_{2i} = \check{\mathbf{X}}_{2i} - \check{\mathbf{X}}_{2di}$, $\bar{\mathbf{E}}_{2i} = \check{\mathbf{X}}_{2di} - \check{\mathbf{X}}_{2ci}$. Choose the Lyapunov function as:

$$V_{c2i} = \frac{1}{2} \check{\check{\mathbf{E}}}_{2i}^T \check{\check{\mathbf{E}}}_{2i} \tag{53}$$

By differentiating (53), one yields:

$$\begin{aligned} \dot{V}_{c2i} &= \check{E}_{2i}^T \dot{\check{E}}_{2i} \\ &= \check{E}_{2i}^T (\dot{\check{X}}_{2i} - \dot{\check{X}}_{2id}) \\ &= \check{E}_{2i}^T (\eta_i \dot{x}_{2i} + \check{\xi}_i - \dot{\check{X}}_{2id}) \\ &= \check{E}_{2i}^T [\eta_i (F_{2i} + G_{2i}u_{0i} + G_{2i}f_{ai} + \dot{f}_{si} + \hat{W}_i) + \check{\xi}_i - \dot{\check{X}}_{2id}] \end{aligned} \tag{54}$$

where $\check{\xi}_i = [\check{\xi}_{i1}, \check{\xi}_{i2}, \check{\xi}_{i3}]^T$, $\check{\xi}_{ih} = (\underline{x}_{2ih} - \bar{x}_{2ih} + 2\hat{x}_{2ih})\hat{x}_{2ih}\check{x}_{2ih} / (\underline{x}_{2ih} + \hat{x}_{2ih})(\bar{x}_{2ih} - \hat{x}_{2ih})^2$, $h = 1, 2, 3$.

Finally, the FTCC law is designed as:

$$\begin{aligned} u_{0i} &= G_{2i}^{-1} [-\hat{F}_{2i} - G_{2i}\hat{f}_{ai} - \dot{f}_{si} - \hat{W}_i + \eta_i^{-1} (\dot{\check{X}}_{2id} - \check{\xi}_i)] \\ &\quad - G_{2i}^{-1} \eta_i^{-1} (G_{1i}K_{1i}A_{1i}e_{1i} + K_{4i}\text{sig}^{2p_i-1}(\check{E}_{2i}) + K_{5i}\text{sig}^{2q_i-1}(\check{E}_{2i}) + 2\eta_i^2 \check{E}_{2i}) \end{aligned} \tag{55}$$

where \hat{F}_{2i} is the nonlinear function containing the estimation of state variables. $\hat{F}_{ai} = G_{2i}\hat{f}_{ai} = [\hat{f}_{ai4}, 0, 0]^T$ is the estimation of the actuator fault. \hat{W}_i is the estimation of \bar{W}_i . $K_{4i} = \text{diag}\{K_{4i1}, K_{4i2}, K_{4i3}\}$ and $K_{5i} = \text{diag}\{K_{5i1}, K_{5i2}, K_{5i3}\}$ are parameter matrices to be designed, $K_{4i1}, K_{4i2}, K_{4i3}, K_{5i1}, K_{5i2}, K_{5i3} > 0$. In conclusion, the developed scheme is shown in Figure 1.

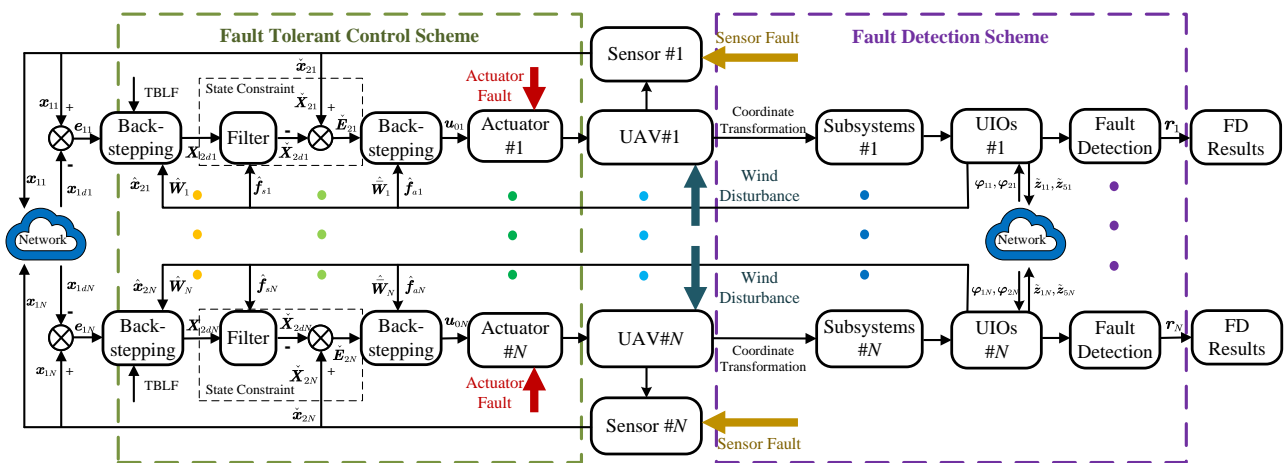


Figure 1. Overall FD and FTCC scheme.

Theorem 2. Consider a group of fixed-wing UAVs (1)–(2) under actuator fault (5), sensor fault (6), and wind disturbances. If the state transformation (46) and TBLF (48) are adopted to keep the state variables and position tracking errors within their constraints, the filter is proposed as (52), the control laws are designed as (50), (51), (55), and, then, the fixed-wing UAVs can keep cooperative formation flight and the errors of the multi-UAVs system are fixed-time convergent.

Proof. Select the Lyapunov function as:

$$V_i = \frac{1}{2} e_{1i}^T A_{1i} e_{1i} + \frac{1}{2} \check{E}_{2i}^T \check{E}_{2i} + \frac{1}{2} \bar{E}_{2i}^T \bar{E}_{2i} \tag{56}$$

By considering (49), (51), (54), (55), differentiating (56), and using Young’s inequality, one yields:

$$\begin{aligned}
 \dot{V}_i &= e_{1i}^T A_{1i} \dot{e}_{1i} + \check{E}_{2i}^T \dot{\check{E}}_{2i} + \bar{E}_{2i}^T \dot{\bar{E}}_{2i} \\
 &= e_{1i}^T A_{1i} [G_{1i} K_{1i} (\check{E}_{2i} + \bar{E}_{2i}) + \tilde{F}_{1i} - G_{1i} \tilde{f}_{si} + \tilde{W}_i] - e_{1i}^T (K_{2i} \text{sig}^{2p_i-1}(e_{1i}) + K_{3i} \text{sig}^{2q_i-1}(e_{1i})) \\
 &\quad + \check{E}_{2i}^T [\eta_i (\tilde{F}_{2i} + G_{2i} \tilde{f}_{ai} + \dot{\tilde{f}}_{si} + \tilde{W}_i)] + \bar{E}_{2i}^T (-\eta_i (\text{sig}^{s_{1i}-1}(\bar{E}_{2i}) + \text{sig}^{s_{2i}-1}(\bar{E}_{2i})) - \frac{1}{2} \bar{E}_{2i}) \\
 &\quad - \bar{E}_{2i}^T \dot{\check{X}}_{2ci} - \check{E}_{2i}^T (K_{4i} \text{sig}^{2p_i-1}(\check{E}_{2i}) + K_{5i} \text{sig}^{2q_i-1}(\check{E}_{2i}) + 2\eta_i^2 \check{E}_{2i}) \\
 &\quad - \check{E}_{2i}^T G_{1i} K_{1i} A_{1i} e_{1i} - \frac{3}{2} e_{1i}^T A_{1i}^2 e_{1i} \\
 &= \bar{E}_{2i}^T (-\eta_i (\text{sig}^{s_{1i}-1}(\bar{E}_{2i}) + \text{sig}^{s_{2i}-1}(\bar{E}_{2i})) - \frac{1}{2} \bar{E}_{2i}) + \bar{E}_{2i}^T (G_{1i} K_{1i} A_{1i} e_{1i} - \dot{\check{X}}_{2ci}) \\
 &\quad + e_{1i}^T A_{1i} (\tilde{F}_{1i} - G_{1i} \tilde{f}_{si} + \tilde{W}_i) - e_{1i}^T (K_{2i} \text{sig}^{2p_i-1}(e_{1i}) + K_{3i} \text{sig}^{2q_i-1}(e_{1i}) + \frac{3}{2} A_{1i}^2 e_{1i}) \\
 &\quad + \check{E}_{2i}^T \eta_i (\tilde{F}_{2i} + G_{2i} \tilde{f}_{ai} + \dot{\tilde{f}}_{si} + \tilde{W}_i) - \check{E}_{2i}^T (K_{4i} \text{sig}^{2p_i-1}(\check{E}_{2i}) + K_{5i} \text{sig}^{2q_i-1}(\check{E}_{2i}) + 2\eta_i^2 \check{E}_{2i}) \\
 &\leq -K_{2i} \|e_{1i}\|^{2p_i} - K_{3i} \|e_{1i}\|^{2q_i} - K_{4i} \|\check{E}_{2i}\|^{2p_i} - K_{5i} \|\check{E}_{2i}\|^{2q_i} - \eta_{2i} \|\bar{E}_{2i}\|^{s_{1i}} - \eta_{2i} \|\bar{E}_{2i}\|^{s_{2i}} \\
 &\quad + \frac{1}{2} (\tilde{F}_{1i}^T \tilde{F}_{1i} + \tilde{f}_{si}^T G_{1i}^2 \tilde{f}_{si} + \tilde{W}_i^T \tilde{W}_i + \tilde{F}_{2i}^T \tilde{F}_{2i} + \tilde{f}_{ai}^T G_{2i}^2 \tilde{f}_{ai} + \dot{\tilde{f}}_{si}^T \dot{\tilde{f}}_{si} + \tilde{W}_i^T \tilde{W}_i + \omega^2)
 \end{aligned} \tag{57}$$

where $\tilde{F}_{1i} = F_{1i} - \hat{F}_{1i}$, $\tilde{F}_{2i} = F_{2i} - \hat{F}_{2i}$, $\tilde{f}_{ai} = f_{ai} - \hat{f}_{ai}$ is the estimation error of f_{ai} , $\tilde{f}_{si} = f_{si} - \hat{f}_{si}$ is the estimation error of f_{si} , ω is a positive constant, which is assumed to satisfy $\|G_{1i} K_{1i} A_{1i} e_{1i} - \dot{\check{X}}_{2ci}\| \leq \omega$.

Further, choosing $p_i = s_{1i}/2$ and $q_i = s_{2i}/2$, one can obtain:

$$\dot{V}_i \leq -\Lambda_{1i} V_i^{p_i} - \Lambda_{2i} V_i^{q_i} + \Lambda_{3i} \tag{58}$$

where $\Lambda_{1i} = \min\{\lambda_{\min}(K_{2i})2^{p_i}, \lambda_{\min}(K_{4i})2^{p_i}, \lambda_{\min}(\eta_{2i})2^{p_i}\}$, $\Lambda_{2i} = \min\{\lambda_{\min}(K_{3i})2^{q_i}, \lambda_{\min}(K_{5i})2^{q_i}, \lambda_{\min}(\eta_{2i})2^{q_i}\}$, $\Lambda_{3i} = \bar{\epsilon}_i$. $\lambda_{\min}(\bullet)$ represents the minimum eigenvalue of the matrix. $\bar{\epsilon}_i$ is assumed to be the upper bound of $\epsilon_i = \frac{1}{2} (\tilde{F}_{1i}^T \tilde{F}_{1i} + \tilde{f}_{si}^T G_{1i}^2 \tilde{f}_{si} + \tilde{W}_i^T \tilde{W}_i + \tilde{F}_{2i}^T \tilde{F}_{2i} + \tilde{f}_{ai}^T G_{2i}^2 \tilde{f}_{ai} + \dot{\tilde{f}}_{si}^T \dot{\tilde{f}}_{si} + \tilde{W}_i^T \tilde{W}_i + \omega^2)$.

According to Lemma 1, the error signals of the multi-UAV system are fixed-time bounded and convergent, wherein V_i can converge to the following set $\left\{ V_i \leq \min \left\{ \left(\frac{\Lambda_{3i}}{(1-\phi_i)\Lambda_{1i}} \right)^{\frac{1}{p_i}}, \left(\frac{\Lambda_{3i}}{(1-\phi_i)\Lambda_{2i}} \right)^{\frac{1}{q_i}} \right\} \right\}$, and the setting time is presented as $T_{ci} \leq T_{ci \max} = \frac{1}{\Lambda_{1i}\phi_i(p_i-1)} + \frac{1}{\Lambda_{2i}\phi_i(1-q_i)}$ with $0 < \phi_i < 1$.

This completes the proof of Theorem 2. \square

5. Simulation Results

The effectiveness of the designed FD and FTCC scheme was verified by means of simulations described in this section. The structure and aerodynamic parameters of fixed-wing UAVs referred to [42]. In the simulations, actuator faults were encountered by UAV#1 at $t = 15$ s and by UAV#2 at $t = 45$ s, respectively. Sensor faults were encountered by UAV#2 at $t = 40$ s and by UAV#4 at $t = 75$ s, respectively. The actuator and sensor faults are given in Table 1. Wind disturbances were encountered by the UAVs at $t = 10$ s in the simulations, $W_y = 0$, $W_z = 0$, and W_x are given in Table 2.

Table 1. Description of sensor and actuator fault models.

	UAV#1	UAV#2	UAV#4
Actuator fault	$\begin{cases} \rho_{t1} = 1, \delta_{tb1} = 0, & t < 15 \text{ s} \\ \rho_{t1} = 0.6, \delta_{tb1} = -0.05, & t \geq 15 \text{ s} \end{cases}$	$\begin{cases} \rho_{t2} = 1, \delta_{tb2} = 0, & t < 45 \text{ s} \\ \rho_{t2} = 0.65, \delta_{tb2} = 0.015, & t \geq 45 \text{ s} \end{cases}$	\
Sensor fault	\	$\begin{cases} \rho_{v2} = 1, V_{b2} = 0, & t < 40 \text{ s} \\ \rho_{v2} = 0.7, V_{b2} = 20, & t \geq 40 \text{ s} \end{cases}$	$\begin{cases} \rho_{v4} = 1, V_{b4} = 0, & t < 75 \text{ s} \\ \rho_{v4} = 0.8, V_{b4} = 3, & t \geq 75 \text{ s} \end{cases}$

Table 2. Description of wind disturbance model.

	$t < 10 \text{ s}$	$10 \text{ s} \leq t < 30 \text{ s}$	$30 \text{ s} \leq t < 60 \text{ s}$	$t \geq 60 \text{ s}$
W_x	0	$-0.1e^{-0.5(t-10)} + 0.1$	$0.4e^{-0.5(t-30)} - 0.3$	$-0.5e^{-0.5(t-60)} + 0.2$

The chosen design control parameters were $T_{max} = 100$, $\eta_{2i} = \text{diag}\{0.6, 0.6, 0.6\}$, $k_b = 0.5$, $x_{2i1} = 0$, $\bar{x}_{2i1} = 32$, $x_{2i2} = 0.2$, $\bar{x}_{2i2} = 0.2$, $x_{2i3} = 0.2$, $\bar{x}_{2i3} = 0.2$, $p_i = 0.95$, $q_i = 1.2$, $s_{1i} = 1.9$, $s_{2i} = 2.4$, $K_{2i} = \text{diag}\{15, 23, 23\}$, $K_{3i} = \text{diag}\{10, 22, 22\}$, $K_{4i} = \text{diag}\{33, 3, 3\}$, $K_{5i} = \text{diag}\{36, 3, 3\}$. The parameters for UIOs are designed as $a_1 = 0.65$, $b_1 = 0.85$, $a_3 = 0.55$, $b_3 = 0.75$, $L_1 = L_2 = 32$, $L_3 = 5$, $L_4 = 6$, $L_5 = 15$, $L_6 = 16$. The parameter for FD was designed as $H_{1i} = 3$. The initial conditions of fixed-wing UAVs were $x_{10}(0) = [0, 0, 0]^T$ m, $x_{11}(0) = [0, 0.01, 1030]^T$ m, $x_{12}(0) = [-0.02, -27, 1012]^T$ m, $x_{13}(0) = [0.02, 27, 1012]^T$ m, $x_{14}(0) = [0.01, -18, 976]^T$ m, $x_{15}(0) = [-0.01, 18, 976]^T$ m, $V_i(0) = 30 \text{ m/s}$, $\gamma_i(0) = 0^\circ$, $\chi_i(0) = 0^\circ$. The expected value of the relative position between fixed-wing UAVs are shown in Table 3. The trajectory of the leader was given by $x_{10} = [30t, 0, 1000]^T$ m. The communication topology of the UAVs is shown in Figure 2. Thus, the Laplacian matrix and leader adjacency matrix could be calculated as:

$$\mathcal{L} = \mathcal{D} - \mathcal{A} = \begin{bmatrix} 0 & 1 & 1 & 1 & 0 \\ 1 & 0 & 1 & 0 & 1 \\ 1 & 1 & 0 & 0 & 0 \\ 1 & 0 & 0 & 0 & 1 \\ 0 & 1 & 0 & 1 & 0 \end{bmatrix} - \begin{bmatrix} 3 & 0 & 0 & 0 & 0 \\ 0 & 3 & 0 & 0 & 0 \\ 0 & 0 & 2 & 0 & 0 \\ 0 & 0 & 0 & 2 & 0 \\ 0 & 0 & 0 & 0 & 2 \end{bmatrix} = \begin{bmatrix} 3 & -1 & -1 & -1 & 0 \\ -1 & 3 & -1 & 0 & -1 \\ -1 & -1 & 2 & 0 & 0 \\ -1 & 0 & 0 & 2 & -1 \\ 0 & -1 & 0 & -1 & 2 \end{bmatrix}, \mathcal{C} = \begin{bmatrix} 1 & 0 & 0 & 0 & 0 \\ 0 & 1 & 0 & 0 & 0 \\ 0 & 0 & 0 & 0 & 0 \\ 0 & 0 & 0 & 0 & 0 \\ 0 & 0 & 0 & 0 & 0 \end{bmatrix}.$$

Solving the matrix inequality (30) by means of the LMI toolbox, matrices P_1 and P_2 could be calculated as:

$$P_1 = 10^{-2} \begin{bmatrix} 1.56 & 0 & 0 & 0 \\ 0 & 1.56 & 0 & 0 \\ 0 & 0 & 0.49 & 2.41 \\ 0 & 0 & 2.41 & -3.78 \end{bmatrix}, P_2 = 10^{-2} \begin{bmatrix} 0.25 & 0 & 0 & 0.23 \\ 0 & 0.26 & 0 & 0 \\ 0 & 0 & 0.26 & 0 \\ 0.23 & 0 & 0 & -6.03 \end{bmatrix}$$

Table 3. Expected value of the relative position between fixed-wing UAVs.

	UAV#1 ($i = 1$)	UAV#2 ($i = 2$)	UAV#3 ($i = 3$)	UAV#4 ($i = 4$)	UAV#5 ($i = 5$)
R_{i0} [m]	$[0, 0, 30]^T$	$[0, -27, 12]^T$	\	\	\
R_{i1} [m]	\	$[0, -27, -18]^T$	$[0, 27, -18]^T$	$[0, -18, -54]^T$	\
R_{i2} [m]	$[0, 27, 18]^T$	\	$[0, 54, 0]^T$	\	$[0, 45, -36]^T$
R_{i3} [m]	$[0, -27, 18]^T$	$[0, -54, 0]^T$	\	\	\
R_{i4} [m]	$[0, 18, 54]^T$	\	\	\	$[0, 36, 0]^T$
R_{i5} [m]	\	$[0, -45, 36]^T$	\	$[0, -36, 0]^T$	\

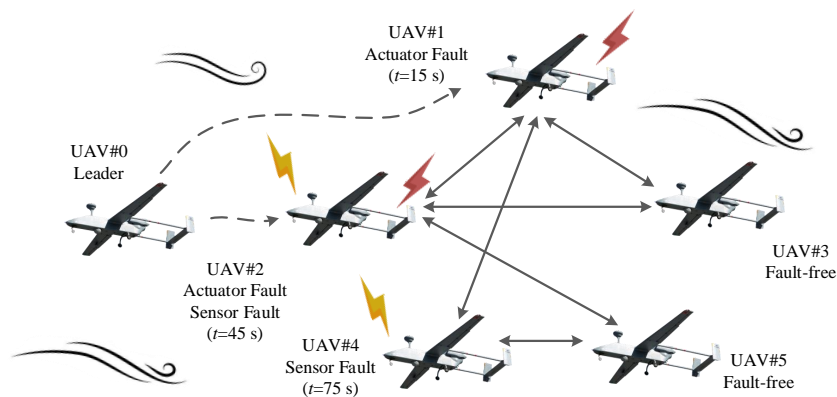


Figure 2. Communication topology.

Figure 3 illustrates the flight paths of multi-UAVs. It can be seen that the fixed-wing UAVs kept cooperative formation flight even if the multi-UAV system was subjected to actuator faults, sensor faults, and wind disturbances. The thrust throttle setting of UAV# i ($i = 1, 2, 3, 4, 5$) is presented in Figure 4. The control inputs enabled a quick response as the faults and disturbances were encountered. Figure 5 demonstrates the generalized position tracking errors of the i th UAV, and it can be observed that the errors were convergent to a neighborhood containing zero. Figure 6 shows the residuals and thresholds of UAV#1, 2, 4 for the FD unit, respectively. It can be seen from the FD results that the residual functions for actuator fault and sensor fault exceeded the corresponding FD thresholds when an actuator fault or a sensor fault occurred. Meanwhile, the residual signals were smaller than the corresponding FD thresholds if no faults occurred. Therefore, the occurrence of actuator and sensor faults could be promptly detected by utilizing the designed FD scheme. The estimations of wind disturbances, airspeed, and faults are demonstrated in Figure 7, Figure 8, and Figure 9, respectively. It can be observed that the developed cooperative UIOs had excellent observation capabilities. The states of the multi-UAV system, disturbances, and faults approximated rapidly and accurately. Furthermore, it was found from the above simulation results that the flight performance of UAVs was affected if neighboring UAVs suffered from faults.

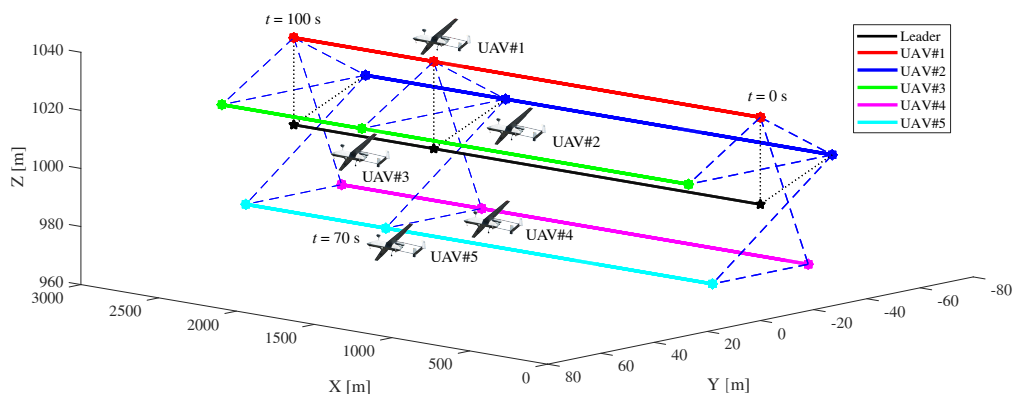


Figure 3. Flight paths of multi-UAVs.

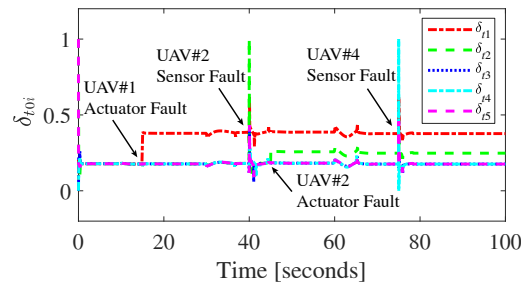


Figure 4. δ_{t0i} of the i th UAV.

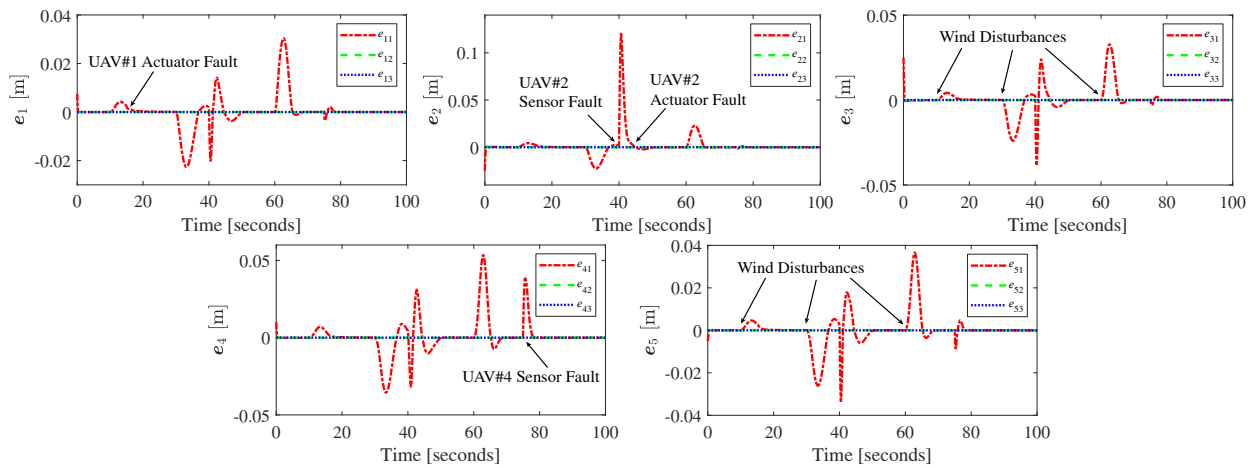


Figure 5. The generalized position tracking errors of the i th UAV.

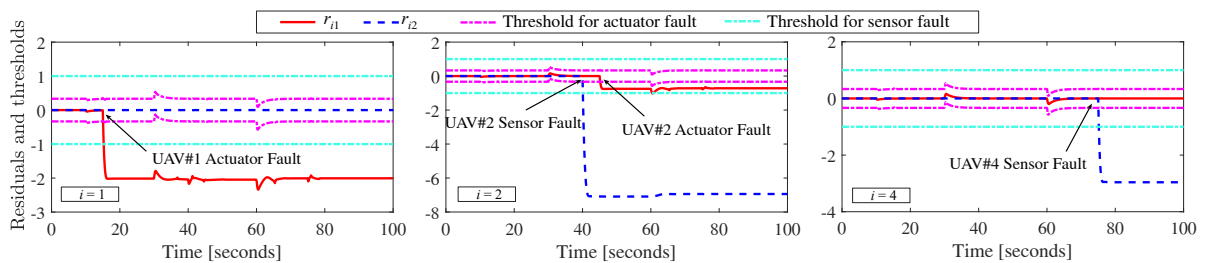


Figure 6. Residuals and thresholds for FD.

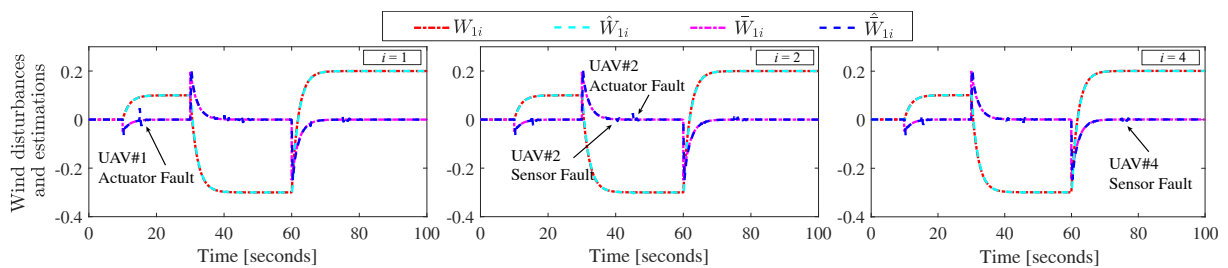


Figure 7. Wind disturbances and estimations.

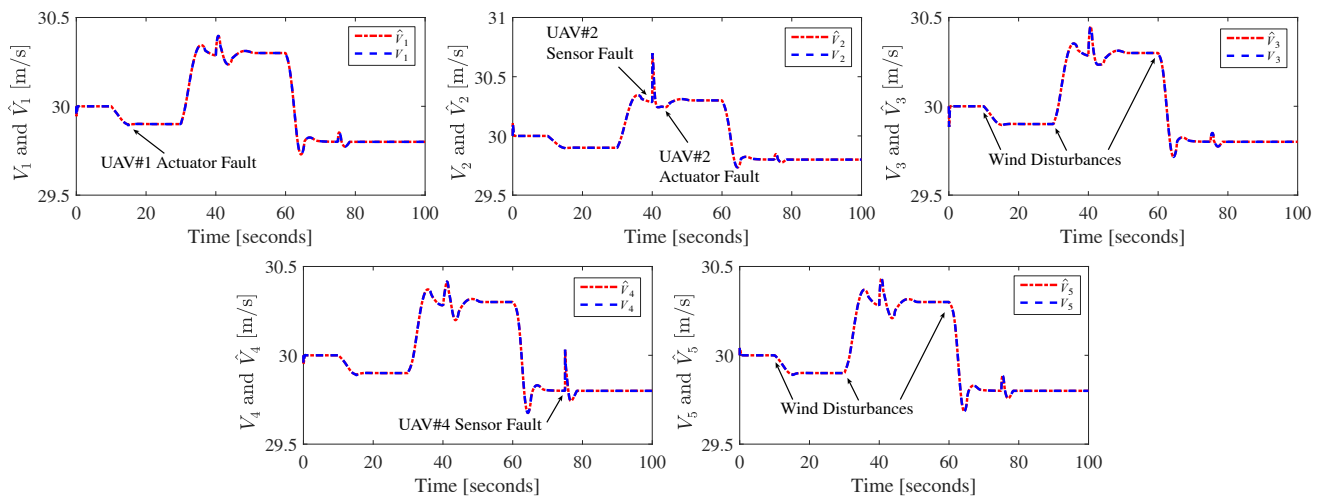


Figure 8. Airspeeds and estimations.

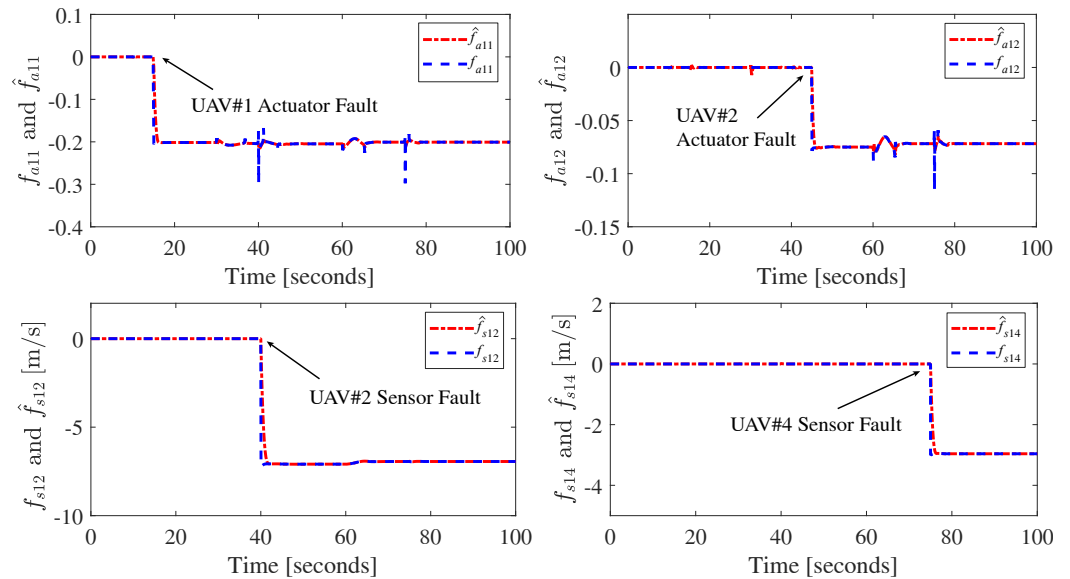


Figure 9. Faults and estimations.

The comparative simulations between the proposed cooperative FD scheme and the individual FD scheme demonstrated the superiority of the proposed scheme. Note that the comparative individual FD scheme was derived by removing cooperative terms, including φ_{1i} and φ_{2i} from the UIOs. Consider the fact that UAV#2 simultaneously encountered actuator and sensor faults, only the generalized position tracking error and estimations of the velocity, faults, and wind disturbances of UAV#2 are presented to show the superiority of the developed method. It can be seen from Figure 10 that the convergence rate of tracking errors under the developed method was faster than the comparative scheme. Therefore, one can conclude that the performance of the developed FD scheme is enhanced by introducing cooperative terms.

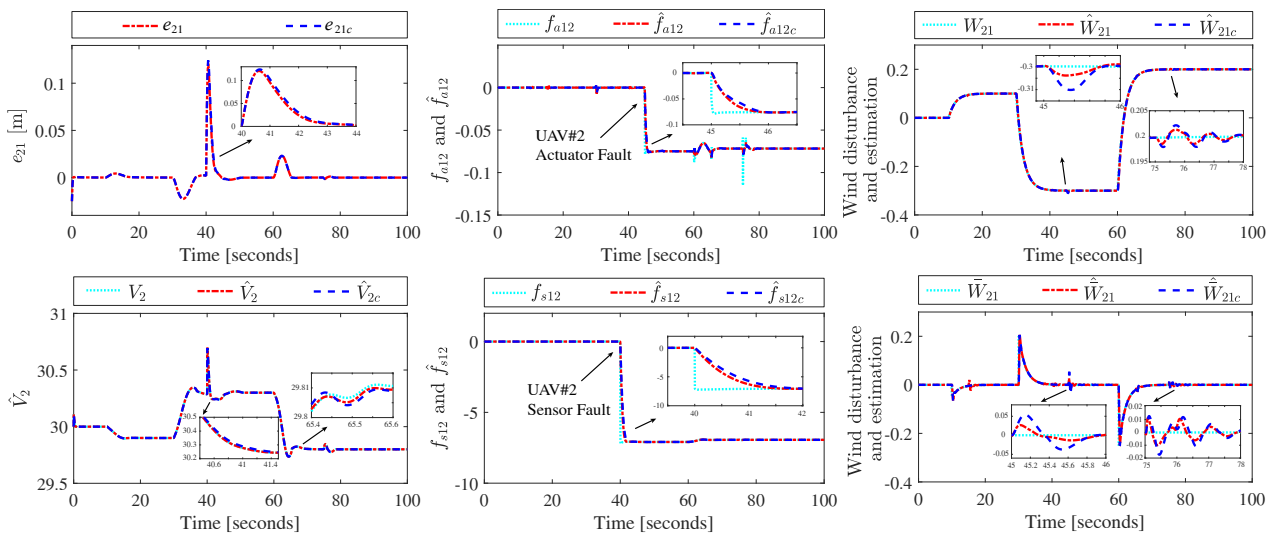


Figure 10. Comparison between the proposed cooperative FD scheme and the individual FD scheme.

6. Conclusion and Future Work

In this study, the FD and FTCC schemes were propounded for multiple fixed-wing UAVs against actuator faults, sensor faults, and wind disturbances. In the FD unit, the faulty UAV model with wind disturbances was linearized and the system was converted into two subsystems by using state and output transformations. Then, cooperative UIOs were developed to estimate the states, faults, and disturbances. The adaptive thresholds were designed to detect actuator and sensor faults by using the observers' estimations. In the FTCC unit, state constraints were considered. Furthermore, backstepping-based fixed-time FTCC laws were proposed for multi-UAVs suffering from actuator faults, sensor faults, and wind disturbances. Lyapunov analysis proved the fixed-time convergence of the tracking errors in the multi-UAV system. The simulation results showed the effectiveness of the FD and FTCC strategies.

In the current study, only the effectiveness loss, deviation of thrust throttle setting, and pitot faults were considered in the FD and FTCC scheme design for the fixed-wing follower UAVs. As one of future works, more actuator and sensor faults, such as actuator stuck faults, will be investigated. Furthermore, the effects of faults and wind disturbances on real UAV testbeds with one leader UAV, or even multiple leader UAVs, will be considered in future research. Eventually, implementation and experimental tests of the proposed scheme on systems with real UAVs will be carried out.

Author Contributions: Conceptualization, Y.C., G.X. and Y.Z.; Methodology, Z.Y. (Zhongyu Yang) and M.L.; Supervision, Z.Y. (Ziquan Yu) and G.X.; Validation, Z.Y. (Zhongyu Yang) and M.L.; Visualization, Z.Y. (Zhongyu Yang); Writing—original draft, Z.Y. (Zhongyu Yang); Writing—review & editing, Z.Y. (Ziquan Yu), Y.C. and Y.Z. All authors have read and agreed to the published version of the manuscript.

Funding: This work was supported in part by the National Natural Science Foundation of China (No. 62003162, 61833013, 62233009), the Natural Science Foundation of Jiangsu Province of China (No. BK20200416, BK20222012), the China Postdoctoral Science Foundation (No. 2020TQ0151, 2020M681590), the Industry–University Research Innovation Foundation for the Chinese Ministry of Education (No. 2021ZYA02005), the Science and Technology on Space Intelligent Control Laboratory (No. HTKJ2022KL502015), the Aeronautical Science Foundation of China (No. 20220007052003, 20200007018001), the Postgraduate Research & Practice Innovation Program of NUAU (No. xcjxh20220325); and the Natural Sciences and Engineering Research Council of Canada.

Data Availability Statement: The data presented in this study are available on request from the corresponding author upon reasonable request.

Conflicts of Interest: The authors declare no conflict of interest.

References

1. Yang, X.S.; Tang, L.B.; Wang, H.S.; He, X.X. Early detection of forest fire based on unmaned aerial vehicle platform. In Proceedings of the IEEE International Conference on Signal, Information and Data Processing, Chongqing, China, 11–13 December 2019.
2. Yfantis, E.A. A UAV with autonomy, pattern recognition for forest fire prevention, and AI for providing advice to firefighters fighting forest fires. In Proceedings of the IEEE 9th Annual Computing and Communication Workshop and Conference, Las Vegas, NV, USA, 7–9 January 2019.
3. Bi, J.T.; Mao, W.B.; Gong, Y.J. Research on image mosaic method of UAV image of earthquake emergency. In Proceedings of the International Conference on Agro-Geoinformatics, Beijing, China, 11–14 August 2014.
4. Li, Z.R.; Liu, Y.; Walker, R.; Hayward, R.; Zhang, J.L. Towards automatic power line detection for a UAV surveillance system using pulse coupled neural filter and an improved Hough transform. *Mach. Vis. Appl.* **2010**, *21*, 677–686. [[CrossRef](#)]
5. Hristov, G.; Raychev, J.; Kinaneva, D.; Zahariev, P. Emerging methods for early detection of forest fires using unmanned aerial vehicles and lorawan sensor networks. In Proceedings of the 28th EAAEIE Annual Conference, Hafnarfjordur, Iceland, 26–28 September 2018.
6. Fahmani, L.; Garfaf, J.; Boukhdar, K.; Benhadou, S.; Medromi, H. Unmanned aerial vehicles inspection for overhead high voltage transmission lines. In Proceedings of the International Conference on Innovative Research in Applied Science, Engineering and Technology, Meknes, Morocco, 16–19 April 2020.
7. Wu, G.F.; Gao, X.G.; Fu, X.W.; Wan, K.F.; Di, R.H. Mobility control of unmanned aerial vehicle as communication relay in airborne multi-user systems. *Chin. J. Aeronaut.* **2019**, *32*, 1520–1529. [[CrossRef](#)]
8. Peng, H.; Shen, L.C.; Zhu, H.Y. Multiple UAV cooperative area search based on distributed model predictive control. *Acta Aeronaut. Astronaut. Sin.* **2010**, *31*, 593–601.
9. No, T.S.; Kim, Y.D.; Tahk, M.J.; Jeon, G.E. Cascade-type guidance law design for multiple-UAV formation keeping. *Aerosp. Sci. Technol.* **2011**, *15*, 431–439. [[CrossRef](#)]
10. Seo, J.B.; Kim, Y.D.; Tsourdos, A.; White, B.A. Multiple UAV formation reconfiguration with collision avoidance guidance via differential geometry concept. In Proceedings of the International Congress of the Aeronautical Sciences ICAS, Brisbane, Australia, 23–28 September 2012; pp. 1–8.
11. Bai, R.G.; Sun, X.; Chen, Q.S.; Quan, X.W. Multiple UAV cooperative trajectory planning based on Gauss pseudospectral method. *J. Astronaut.* **2014**, *35*, 1022–1029.
12. Yu, Z.Q.; Zhang, Y.M.; Qu, Y.H. Prescribed performance-based distributed fault-tolerant cooperative control for multi-UAVs. *Trans. Inst. Meas. Control* **2019**, *41*, 975–989. [[CrossRef](#)]
13. Chi, C.Z.; Su, L.; Lyu, Y.X.; Shi, J.P.; Huang, S. Research on real-time fault detection of UAV flight control system sensor based on Riemannian manifold. In *Advances in Guidance, Navigation and Control: Proceedings of 2022 International Conference on Guidance, Navigation and Control, Harbin, China, 5–7 August 2022*; Springer: Berlin/Heidelberg, Germany, 2023; pp. 1219–1227.
14. Grehan, J.; Ignatyev, D.; Zolotas, A. Fault detection in aircraft flight control actuators using support vector machines. *Machines* **2023**, *11*, 211. [[CrossRef](#)]
15. Al-Haddad, L.A.; Jaber, A.A. An intelligent fault diagnosis approach for multirotor UAVs based on deep neural network of multi-resolution transform features. *Drones* **2023**, *7*, 82. [[CrossRef](#)]
16. Liu, Z.B.; Wang, L.N.; Song, Y.C.; Dang, Q.Q.; Ma, B.D. Fault diagnosis and accommodation for multi-actuator faults of a fixed-wing unmanned aerial vehicle. *Meas. Sci. Technol.* **2022**, *33*, 075903. [[CrossRef](#)]
17. Zhang, J.; Swain, A.K.; Nguang, S.K. Robust sensor fault estimation scheme for satellite attitude control systems. *J. Frankl. Inst.* **2013**, *350*, 2581–2604. [[CrossRef](#)]
18. Wu, Y.K.; Jiang, B.; Lu, N.Y.; Yang, H.; Zhou, Y. Multiple incipient sensor faults diagnosis with application to high-speed railway traction devices. *ISA Trans.* **2017**, *67*, 183–192. [[CrossRef](#)]
19. Yin, S.; Gao, H.J.; Qiu, J.B.; Kaynak, O. Descriptor reduced-order sliding mode observers design for switched systems with sensor and actuator faults. *Automatica* **2017**, *76*, 282–292. [[CrossRef](#)]
20. Atallah, M.; Okasha, M.; Dief, T.N.; Jallad, A.H. Optimal consensus control for multi-satellite assembly in elliptic orbit with input saturation. *Acta Astronaut.* **2023**, *208*, 82–90. [[CrossRef](#)]
21. Yu, Y.S.; Shi, C.B.B.; Shan, D.; Lippiello, V.; Yang, Y. A hierarchical control scheme for multiple aerial vehicle transportation systems with uncertainties and state/input constraints. *Appl. Math. Model.* **2022**, *109*, 651–678. [[CrossRef](#)]
22. Chen, Q.J.; Jin, Y.Q.; Wang, T.Y.; Wang, Y.; Yan, T.L.; Long, Y.F. UAV formation control under communication constraints based on distributed model predictive control. *IEEE Access* **2022**, *10*, 126494–126507. [[CrossRef](#)]
23. Aliyari, M.; Wong, W.K.; Bouteraa, Y.; Najafinia, S.; Fekih, A.; Mobayen, S. Design and implementation of a constrained model predictive control approach for unmanned aerial vehicles. *IEEE Access* **2022**, *10*, 91750–91762. [[CrossRef](#)]
24. Yan, K.; Wu, Q.X. Adaptive tracking flight control for unmanned autonomous helicopter with full state constraints and actuator faults. *ISA Trans.* **2022**, *128*, 32–46. [[CrossRef](#)]
25. Wang, Z.X.; Yang, P.; Hu, X.K.; Zhang, Z.Q.; Wen, C.W. Sliding mode fault tolerant control of quadrotor UAV with state constraints under actuator fault. *Int. J. Innov. Comput. I* **2021**, *17*, 639–653.
26. Zhang, B.Y.; Sun, X.X.; Lv, M.L.; Liu, S.G.; Li, L. Distributed adaptive fixed-time fault-tolerant control for multiple 6-DOF UAVs with full-state constraints guarantee. *IEEE Syst. J.* **2021**, *16*, 4792–4803. [[CrossRef](#)]

27. Li, Z.; Chen, X.; Xie, M.Y.; Zhao, Z.H. Adaptive fault-tolerant tracking control of flying-wing unmanned aerial vehicle with system input saturation and state constraints. *Trans. Inst. Meas. Control* **2022**, *44*, 880–891. [[CrossRef](#)]
28. Zhou, Y.; Dong, W.H.; Liu, Z.C.; Lv, M.L.; Zhang, W.Q.; Chen, Y. IBLF-based fixed-time fault-tolerant control for fixed-wing UAV with guaranteed time-varying state constraints. *IEEE Trans. Veh. Technol.* **2022**, *72*, 4252–4266. [[CrossRef](#)]
29. Jin, X. Fault tolerant finite-time leader–follower formation control for autonomous surface vessels with LOS range and angle constraints. *Automatica* **2016**, *68*, 228–236. [[CrossRef](#)]
30. Li, J.Q.; Kumar, K.D. Fault tolerant attitude synchronization control during formation flying. *J. Aerosp. Eng.* **2011**, *24*, 251–263. [[CrossRef](#)]
31. Zhang, J.X.; Yang, G.H. Fault-tolerant leader–follower formation control of marine surface vessels with unknown dynamics and actuator faults. *Int. J. Robust Nonlinear Control* **2018**, *28*, 4188–4208. [[CrossRef](#)]
32. Cui, B.; Zhao, C.H.; Ma, T.D.; Feng, C. Distributed adaptive neural network control for a class of heterogeneous nonlinear multi-agent systems subject to actuation failures. *Int. J. Syst. Sci.* **2017**, *48*, 559–570. [[CrossRef](#)]
33. Zhou, N.; Xia, Y.Q. Distributed fault-tolerant control design for spacecraft finite-time attitude synchronization. *Int. J. Robust Nonlinear Control* **2016**, *26*, 2994–3017. [[CrossRef](#)]
34. Yu, Z.Q.; Zhang, Y.M.; Liu, Z.X.; Qu, Y.H.; Su, C.Y. Distributed adaptive fractional-order fault-tolerant cooperative control of networked unmanned aerial vehicles via fuzzy neural networks. *IET Contr. Theory Appl.* **2019**, *13*, 2917–2929. [[CrossRef](#)]
35. Wu, Z.H.; Zheng, S.P. Fixed-time fault-tolerant tracking control of fixed-wing UAVs with actuator fault and unmatched disturbances. *Int. J. Aerosp. Eng.* **2022**, *2022*. [[CrossRef](#)]
36. Han, B.; Jiang, J.; Yu, C.J.; Cao, T. Distributed fault estimation and fixed-time fault-tolerant formation control for multi-UAVs subject to sensor faults. *J. Intell. Robot. Syst.* **2022**, *105*, 80. [[CrossRef](#)]
37. Yu, Z.Q.; Zhang, Y.M.; Jiang, B.; Su, C.Y.; Fu, J.; Jin, Y.; Chai, T.Y. Fractional-order adaptive fault-tolerant synchronization tracking control of networked fixed-wing UAVs against actuator-sensor faults via intelligent learning mechanism. *IEEE Trans. Neural Netw. Learn. Syst.* **2021**, *32*, 5539–5553. [[CrossRef](#)]
38. Shao, S.Y.; Chen, M.; Shi, P. *Robust Discrete-Time Flight Control of UAV with External Disturbances*; Springer: Berlin/Heidelberg, Germany, 2021; Volume 317.
39. Cui, G.Z.; Yang, W.; Yu, J.P.; Li, Z.; Tao, C.B. Fixed-time prescribed performance adaptive trajectory tracking control for a QUAV. *IEEE T. Circuits-II* **2021**, *69*, 494–498. [[CrossRef](#)]
40. Yan, X.G.; Edwards, C. Sensor fault detection and isolation for nonlinear systems based on a sliding mode observer. *Int. J. Adapt. Control Signal Process.* **2007**, *21*, 657–673. [[CrossRef](#)]
41. Lv, M.L.; Yu, W.W.; Cao, J.D.; Baldi, S. Consensus in high-power multiagent systems with mixed unknown control directions via hybrid nussbaum-based control. *IEEE T. Cybern.* **2020**, *52*, 5184–5196. [[CrossRef](#)]
42. Lin, W. Distributed UAV formation control using differential game approach. *Aerosp. Sci. Technol.* **2014**, *35*, 54–62. [[CrossRef](#)]

Disclaimer/Publisher’s Note: The statements, opinions and data contained in all publications are solely those of the individual author(s) and contributor(s) and not of MDPI and/or the editor(s). MDPI and/or the editor(s) disclaim responsibility for any injury to people or property resulting from any ideas, methods, instructions or products referred to in the content.